Uplift history of the Troodos ophiolite inferred from integrating thermomechanical models, submarine and deltaic fan clast content and serpentinites

Demi Schutte

6089798

January 2024

Acknowledgements

I would like to thank both my supervisors for their time, help and discussions. Secondly, I would like to thank the Olaf Schuiling fund for their financial contribution to the mineralogy part of this study. I would also like to thank the Molengraaff fund for their financial support of the fieldwork.

Abstract

Uplift of the Troodos ophiolite from its time of formation (~90 Ma) to the present-day is currently poorly constrained, due to its complex multi-phase uplift history involving multiple uplift mechanisms. The aim of this study is to quantify the amount of uplift and uplift rates in the different phases, to construct a more complete timeline of the uplift phases and their mechanisms. The recent (9-0 Ma) uplift history of the Troodos is investigated through analysis of clast content and clast characteristics of submarine and deltaic fans. Thermomechanical models are run to evaluate through which mechanisms serpentinization can contribute to uplift. Serpentinite samples from the Troodos are studied to put temporal constraints on serpentinization. The four formations studied in the fans show four different uplift phases, with uplift rates ranging from 0.025 to 0.4 cm/yr, resulting in 5.8-10.4km total uplift in the past 9Ma. The uplift phases are interpreted to have resulted from regional tectonics: major changes in plate motion, modern subduction initiation and the underthrusting of the Eratosthenes Seamount. The models show 1-12.5 km uplift after 10 myr and uplift rates ranging from 0.1-0.9 cm/yr. In the models, thick or light serpentinite wedges create higher topography compared to thin or dense serpentinite wedges. Erosion decreases the amount of uplift in models with a shallow slab, but it increases the amount of uplift in models with a steep slab, when comparing those models to the ones without erosion. Uplift in the models usually lasts 2-5 million years, before subsidence starts. Steep slab models generally experience less subsidence when erosion is applied. Interpretation of the models show that serpentinite can contribute to uplift by enabling decoupling, as serpentinite has a weak rheology and lowers the frictional strength of a rock. Its buoyancy helps to maintain the already formed topography. The serpentinite samples show a high degree of serpentinization, with very few relict minerals. The serpentine minerals present are predominantly lizardite and minor chrysotile. The most prevalent non-serpentine mineral is magnetite. The samples are interpreted to have formed between 200-400^{0}C in close proximity to the spreading ridge. Previous studies have found antigorite and meteoric indicators in the serpentinite, implying at least three serpentinization phases. The models and field data are then combined to infer the uplift history of the Troodos ophiolite. It seems likely that serpentinization has aided early obduction of the Troodos crust, by necking, breaking and providing buoyancy. This enabled transport of the ophiolitic crust across the subduction zone. After this first period of uplift, a period of relative tectonic quiescence followed, and uplift resumed in the Miocene with the four uplift phases inferred from the fans.

Table of contents

1. Introduction

Ophiolites are rock assemblages that are recognized as remnants of oceanic lithosphere. A French mineralogist was the first to use the term 'ophiolite' to describe serpentinites in 1813 (Brongniart, 1813), after which the definition of an ophiolite was revised to put emphasis on the observation that peridotite, gabbro, diabase and deep-sea sedimentary rocks are often found side-by-side in the Mediterranean mountains (Steinmann, 1927). The plate tectonic theory in the 1960s helped provide a framework for Earth scientists to explain the different characteristics of an ophiolite, after which they were quickly interpreted as fragments of oceanic lithosphere that were found as allochthonous blocks or thrust sheets in mountain ranges (Dilek, 2003; Hess, 1965). An important event in the evolution of the definition of an ophiolite was the Penrose Conference in 1972, in which the signature stratigraphy of an ophiolite was proposed (Dilek, 2003). At the same time, the term 'obduction' was used for the first time to describe a mechanism of emplacement, which was needed to provide an explanation for the dense oceanic lithosphere being uplifted, transported and then emplaced onto the margin of the less dense subducting plate (Coleman, 1971). Contact of an ophiolite with the rocks underneath is often tectonic, which is demonstrated by metamorphic soles (Juteau, 2003). The metamorphic sole characteristically consists of thin sheets (<500m) of predominantly metamorphosed oceanic rocks and minor metamorphosed sedimentary rocks (Wakabayashi & Dilek, 2000). Ophiolites are a valuable source of information to geologists as the rocks provide insight into the oceanic crust and therefore help to improve understanding of petrological, seismic and geological processes within the not easily sampled oceanic lithosphere (Hawkins, 2003).

The eastern Mediterranean hosts multiple ophiolites (figure 1), which have been described as having a near-complete Penrose type stratigraphy, with a cover of pelagic sediments and lacking pyroclastic and volcaniclastic rocks (Dilek, 2003). The Mediterranean ophiolites are underlain by metamorphic soles and mélanges made of ophiolitic and carbonate material, although most Mediterranean metamorphic soles are incomplete and/or dismembered (Dilek, 2003; Inwood et al., 2009; Searle & Cox, 2002). The mantle material is mostly harzburgite and harzburgite-lherzolite (Dilek, 2003). One of those Mediterranean ophiolites is the well-preserved Troodos ophiolite, situated in central Cyprus (figure 1), which shows the complete mantle and crustal sequence (Cann, 2003). The ophiolite's peak, Mount Olympus, is the highest point on the island and made up of serpentinites and partially serpentinized harzburgites and dunites (figure 2). Following the topography downslope reveals the entire ophiolitic crust, consisting of gabbro, plagiogranite, the sheeted dyke complex, pillow lavas, and a sedimentary cover containing umbers and limestones (Bailey et al., 2000). The complete sequence is 8-10 km thick (Ring & Pantazides, 2019).

1.1 Problem statement and aim

From the time of formation of the crust in the Cretaceous to the present-day, the ophiolite has been uplifted in multiple uplift phases (McCallum, 1989). As the specific geodynamic mechanisms that enable the process of obduction remain enigmatic, the mechanisms of Late Cretaceous Troodos ophiolite uplift remain poorly constrained as well. As the Troodos ophiolite lacks a coherent metamorphic sole, some have proposed that obduction has not transpired and instead, other mechanisms such as serpentinization and isostatic readjustment must have contributed to uplift (Evans et al., 2021). Others have interpreted the chaotic mélange of volcanic, sedimentary and serpentinite rocks of the Mamonia Complex as a dismembered sole (Chan et al., 2007; Malpas et al., 1992). As a result of the incoherent nature of the Mamonia Complex, the timing of activity on this supposed sole is poorly constrained as well. Therefore multiple periods of activity have been suggested: 1) between 90 and 83 Ma, based on Ar-Ar data (Bailey et al., 2000; Spray & Roddick, 1981); 2) between 85 and 70 Ma ago, based on the radiolarian ages of the umbers and the

overlying Lefkara formation (Blome & Irwin, 1985); and 3) between 70-65 Ma, based on comparison with other Mediterranean ophiolites and K-Ar data (Whitechurch et al., 1984). Juxtaposition of the Troodos with the Mamonia Complex is supposed to have happened before the end of the Maastrichtian, as they are covered with the same pelagic sediment of the Lefkara Fm (Bailey et al., 2000). Another point of debate remains the margin on which the Troodos would have been obducted, as both the northern margin (Robertson & Woodcock, 1980) and the southern Afro-Arabian margin (Şengör & Yilmaz, 1981; Whitechurch et al., 1984) have been proposed. Spreading ridge mechanisms that have been proposed for early (Cretaceous) uplift are serpentinite diapirism (Schuiling, 2011) and detachment faulting, creating a core complex (Nuriel et al., 2009).

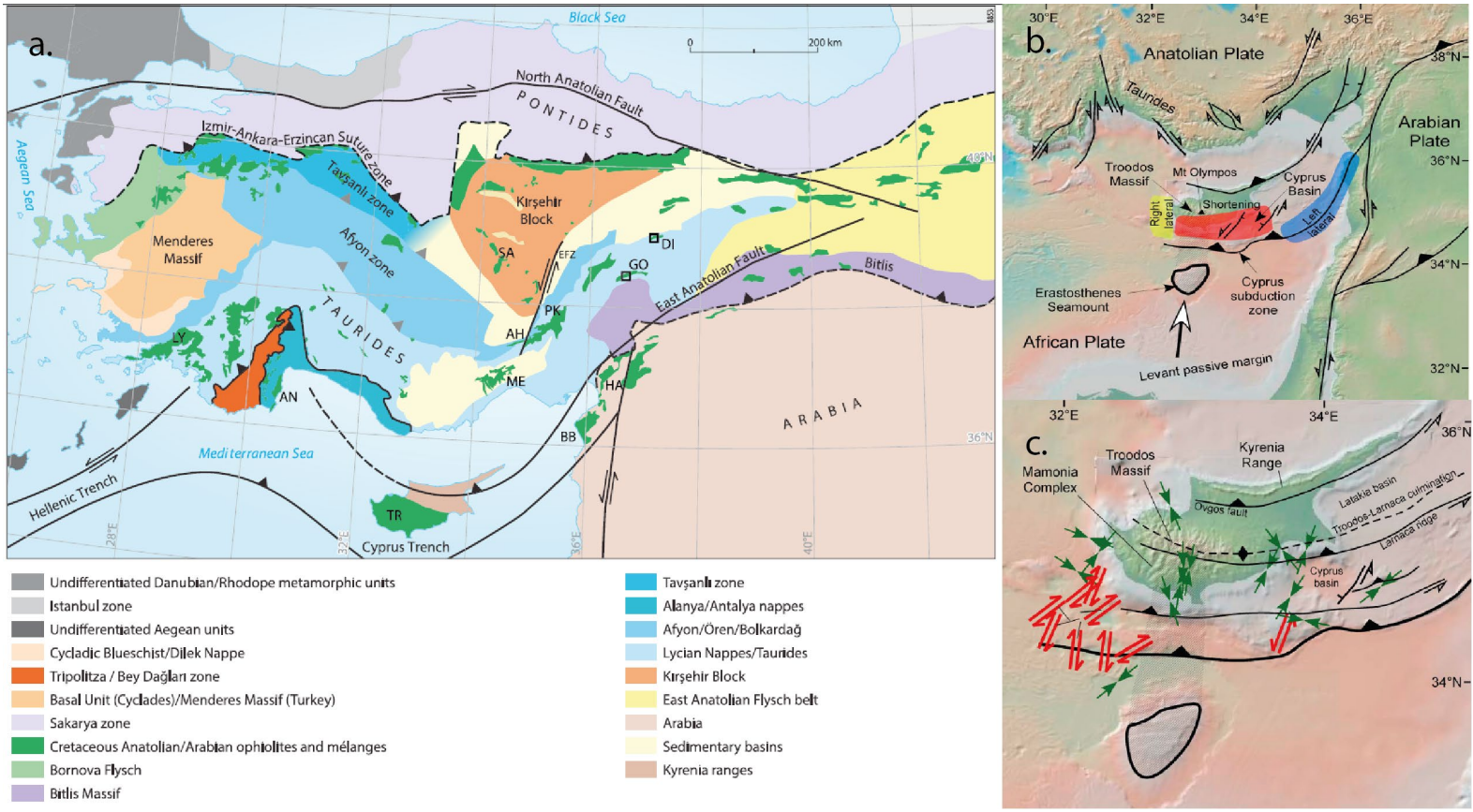

Figure 1 - A. Map of the eastern Mediterranean showing the main tectonic structures and stratigraphic domains in the region. Areas in dark-green are Cretaceous ophiolites and mélanges. After: Maffione et al. (2017). B. Map of the main tectonic regimes and tectonic structures in the Cyprean area. The Eratosthenes seamount, on the Levant passive margin, is located to the south of the island. After: (Ring and Pantazides 2019). C. Map showing main faults and main structural domains on the island of Cyprus and in the trench. After: (Ring and Pantazides 2019)

There is consensus on the occurrence of recent (Neogene and Quaternary) uplift of the Troodos, as inferred from the circum-Troodos sediments. Serpentinite diapirism is an often-suggested mechanism (Evans et al., 2021; Morag et al., 2016) to explain uplift of the Troodos due to the central and topographically high position of serpentinites on the island and their anticlinal structure, but the timing and setting of the Troodos serpentinites are poorly constrained. Some have suggested serpentinite diapirism to be triggered by Miocene initiation of the current subduction zone, as zircon and apatite ages of Troodos rocks suggest rapid exhumation from 6 ± 2 Ma (Morag et al., 2016). Serpentinization is also suggested to be a result of underthrusting of the Eratosthenes seamount at 2Ma, as the serpentinites show an evaporitic signature (Poole & Robertson, 1991; Robertson, 1990, 1998a, 1998b). The evaporitic signature is interpreted to have

come from fluids in the subducted Messinian evaporites of the seamount that have penetrated and hydrated the overlying mantle wedge (Robertson, 1990). In this scenario, serpentinization is a late Cenozoic phenomenon related to subduction. This contrasts with those that have suggested a Cretaceous age for the serpentinites (Nuriel et al., 2009; Schuiling, 2011). Multiple models suggest that serpentinite diapirism is not the primary uplift mechanism (e.g. Ring & Pantazides, 2019). An argument for this is that the buoyancy of the serpentinite is not sufficient to exhume the entire ophiolite to its present position (Shelton, 1993). However, 1D analytical models of the Troodos have shown that it is possible to exhume 17.5km of rocks solely through serpentinization and subsequent isostatic uplift in the last 5.5Ma (Evans et al., 2021). Models that do not incorporate serpentinization as the primary uplift mechanism, suggest that the Eratosthenes seamount has exhumed the Troodos ophiolite by underthrusting, causing crustal thickening and N-S directed shortening (Ben-Avraham et al., 1988; Calon et al., 2005; Ring & Pantazides, 2019). The shortening has created a WNW trending anticline with serpentinite at its core, which is interpreted from N-S striking normal faults (Ben-Avraham et al., 1988; Calon et al., 2005; Ring & Pantazides, 2019). There is consensus on the Eratosthenes seamount having contributed to recent uplift of the Troodos, but through which mechanisms remains unclear. The different mechanisms and hypotheses for uplift point to a complex tectonic evolution of the Troodos ophiolite, with uplift phases that are currently poorly constrained.

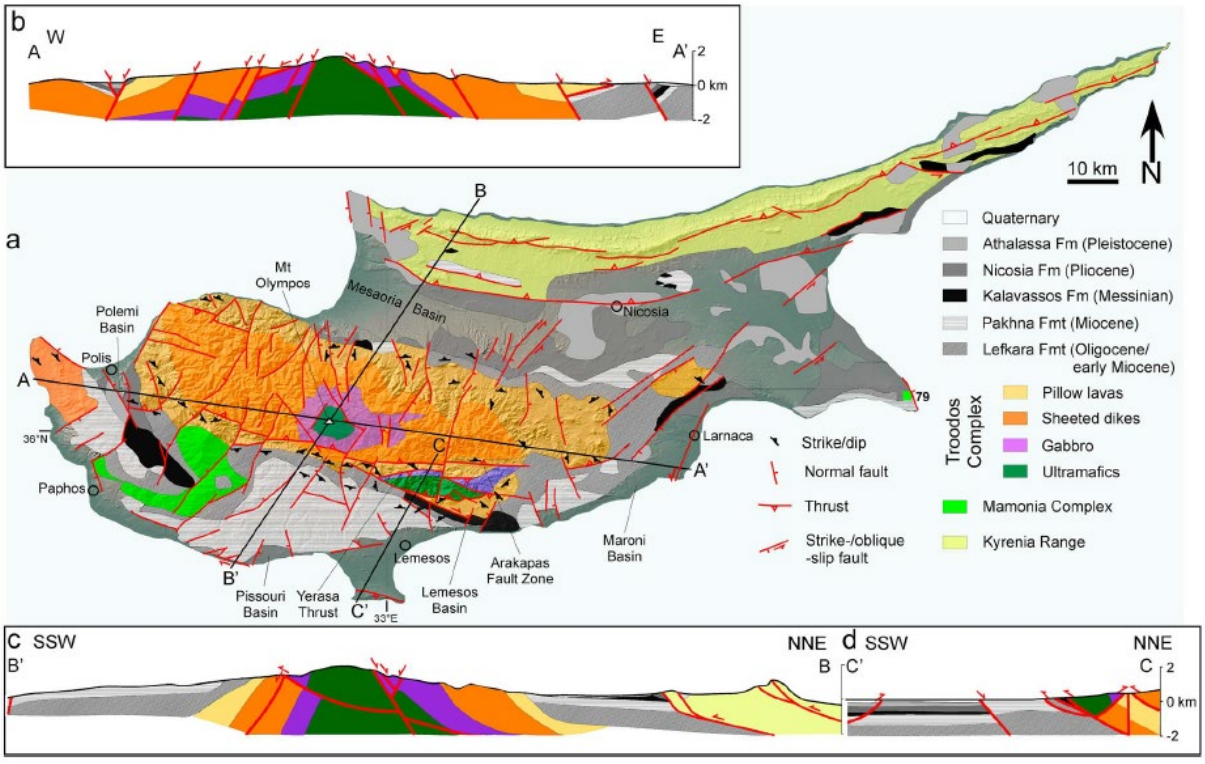

Figure 2 - Geological map of Cyprus, showing the geology of the Troodos in the centre of the island. The map also shows the different basins and large-scale faults on the island. After: (Ring & Pantazides, 2019).

The aim of this study is therefore to quantify the amount of uplift and the uplift rates for the different phases of uplift that have contributed to the exhumation of the Troodos ophiolite, with an emphasis on serpentinization. Submarine and deltaic fans deposited in the last 9 Ma are studied to quantify recent uplift and uplift rates. A parametric thermomechanical modelling exercise is conducted to quantify uplift of an ophiolite in a subduction zone setting and to comprehend to what extent and through which mechanisms serpentinite can contribute to uplift. Samples of the serpentinites are collected to put temporal and tectonic constraints on the serpentinization

process. The field data and model results are then combined to quantify the uplift rates for the various uplift phases of the Troodos ophiolite. With this study we add temporal constraints on the uplift and serpentinization processes in the Troodos ophiolite, to provide a more comprehensive timeline of uplift and its mechanisms over the past ~90 Ma.

1.2 Tectonic setting

1.2.1 General description

The eastern Mediterranean is bordered by the Aegean subduction zone to the west, the Anatolian plateau to the north, the Arabian plate to the east and the African plate to the south (figure 1). Large scale-plate movement is the collision between the African and Eurasian plate, in which the African plate is subducting underneath Eurasia (Reilinger et al., 1997). The two plates have been colliding since the Late Cretaceous (Robertson, 1998b). The plate boundary runs through the eastern Mediterranean (Robertson, 1998b). In the region, the oceanic floor shows a west to east transition from Mesozoic oceanic crust to passive continental margin, which is called the Levant platform (figure 1b) and contains the Eratosthenes seamount (Robertson, 1998b).

Within this overarching framework, Cyprus is located on the Eurasian active margin (figure 1b). There is a subduction zone to the south of Cyprus, where the Eratosthenes seamount is subducting (Robertson, 1998b). Due to its position in the eastern Mediterranean, Cyprus currently functions as a transition zone from extension in the Hellenic arc to strike-slip escape tectonics of the Anatolian microplate in the north (Ben-Avraham et al., 1988). This transition is shown in the tearing of the African slab between the Hellenic arc and Cyprus (Berk Biryol et al., 2011). The subduction zone south of Cyprus is not as active in plate motion and seismicity as the Hellenic arc, as the trench is in transition to continental collision (Ergün et al., 2005; Feld et al., 2017). The Benioff zone is absent in the Cyprean trench, but the slab has not detached yet (Feld et al., 2017; Harrison et al., 2004).

Cyprus has formed by the fusion of the Mamonia Complex, the Kyrenia Range and the Troodos ophiolite (figure 1c, Ring & Pantazides, 2019). The Troodos is 88x29km and covers a third of the island's surface. It includes the Arakapas fault zone in the south-eastern Limassol forest, which has been interpreted as a fossil oceanic transform fault (Murton & Cass, 1986). The Mamonia complex consists of Triassic to Cretaceous volcanic and sedimentary rocks that have been interpreted as a metamorphosed passive margin (figure 1 and 2, Bailey et al., 2000). The Oligocene Kyrenia range is a 20km wide fold-and-thrust belt, consisting of mostly Cretaceous mafic rocks and Permian to middle Miocene sedimentary rocks (figure 1c, McPhee & van Hinsbergen, 2019). The Kyrenia range is interpreted as an island arc (McPhee & van Hinsbergen, 2019).

1.2.2 Geologic history

Cretaceous to Paleogene tectonics

Subduction of the African oceanic lithosphere, i.e. the Neo-Tethys, underneath the Eurasian plate started in the Cretaceous, as the relative plate motions became convergent (Dewey et al., 1989; Feld et al., 2017; Livermore et al., 1984). Within this Neo-Tethyan subduction system, multiple NNE-SSW striking subduction zones formed, in which approximately perpendicular suprasubduction spreading centres were created (MacLeod et al., 2013; Maffione et al., 2017). The Mediterranean ophiolites were all formed within these suprasubduction spreading centres (Maffione et al., 2017). The subducting African plate is thought to have dipped to the east (Woelki et al., 2019).

U-Pb ages of zircons from plagiogranites, zircon (U/Th)/He and apatite fission track cooling ages of Troodos mafic rocks indicate a Late Cretaceous spreading age, approximately at ~90 Ma (Morag

et al., 2016; Mukasa & Ludden, 1987). The cooling ages also indicate that the Troodos spreading axis quickly became cold after formation of the crust, showing that magmatism, roll-back and subduction all were temporary (<10 Ma) processes (Morag et al., 2016). The Troodos crust is thought to have been created from different magma sources, as the inferred original mantle materials show different chemical signatures (Batanova & Sobolev, 2000).

After formation of the crust, from the late Cretaceous until the early Eocene, Cyprus underwent a $\sim 90^0$ counterclockwise rotation, which has been recorded by paleomagnetic data (Clube & Robertson, 1986; Morris, 1996). The rotation most likely happened through oblique subduction of the oceanic crust and ultimately separated Cyprus from Turkey (Clube & Robertson, 1986; Morris, 1996). The rotation is interpreted to not have caused significant uplift (Morag et al., 2016).

The Mamonia Complex

The Mamonia Complex contains Triassic to Cretaceous sedimentary and mafic rocks, and it also hosts tectonic windows through which the post-Cretaceous cover can be seen (Lapierre et al., 2007). The Triassic volcanic rocks are interpreted as remnants of ocean island basalt-type oceanic crusts, including seamounts (Lapierre et al., 2007). In the southwest of Cyprus, the Mamonia Complex meets the Troodos: here, the two are juxtaposed with a chaotic mélange of serpentinized harzburgites, metamorphic rocks and Troodos rocks (Lapierre et al., 2007). The origin and history of the Mamonia Complex remains topic of discussion. It has been interpreted as a tectonic suture zone between the Troodos microplate and a passive margin sequence of Triassic age (Bailey et al., 2000).

Multiple events are recognized in the Mamonia: 1) a strike-slip phase, inducing local metamorphism (c. 90-83 Ma); 2) transtensional deformation associated with the anticlockwise rotation of the Troodos microplate, resulting in retrograde hydration of rocks and emplacement of resulting serpentinites (c. 83-73 Ma); 3) contractional deformation until the end of the Maastrichtian (c. 65 Ma) during which the emplaced serpentinites were reactivated (Bailey et al., 2000). The Troodos and the Mamonia complex are covered by the same Late Cretaceous to Quaternary sediments, starting with the Lefkara Fm (section 1.2.3) (Lapierre et al., 2007).

Neogene tectonics

In the late Miocene (~9 Ma), the motion of the African plate changed, resulting in a change to contractional and strike-slip deformation (Dewey et al., 1989; Harrison et al., 2004). From 9 to 5 Ma, the tectonic style was dominated by transpressive strike-slip faulting (Harrison et al., 2004). The Yerasa fold and thrust belt (figure 2) is considered to be of Miocene age as it is suggested to be related to initiation of the current subduction zone (Eaton & Robertson, 1993). Basin formation in the late Miocene is interpreted to be the result of roll-back of the African slab (Kinnaird & Robertson, 2013).

The tectonic style changed to north-south contractional deformation from 5 Ma to the early Pleistocene (Harrison et al., 2004). During this latter period, the westward escape of Antolia reactivated previously formed structures, resulting in the creation of positive flower structures (Symeou et al., 2018).

In the early Pleistocene, estimated at ~2 Ma, the Eratosthenes seamount enters the Cyprean trench (Kinnaird et al., 2011; Robertson, 1998b). The Eratosthenes seamount is a carbonate platform on the edge of the African plate, supposedly formed on a rifted continental fragment (Ring & Pantazides, 2019). Its basement is unknown (Robertson, 1998b).

1.2.3 Sedimentary geology

Cretaceous

The oldest sediments found in the Circum-Troodos sedimentary cover are of Santonian age and exist of deepwater pelagic sediments, called the Perapedhi formation (Robertson, 1977). These are overlain by the Campanian volcanogenic Kannaviou formation, after which sedimentation returns to deepwater pelagic deposits of the lower Lefkara unit in the Maastrichtian (figure 2 and 3, Robertson, 1977). The Lefkara formation is interpreted to be deposited after emplacement of the crust (Blome & Irwin, 1985).

Paleogene

The sedimentation in the Paleocene is characterised by a gradual shallowing of the seas, which resulted in deposition of calciturbidites (Robertson, 1977). Seas to the north of the Troodos Massif were shallower than to the south (Robertson, 1977). Chalk deposition persisted throughout the middle Eocene, in which the strongly bioturbated rocks of the middle Lefkara were deposited (Robertson, 1977). The deposits are relatively thin on the northern margins of the massif whereas they are thick on the southern side (Robertson, 1977). In the Oligocene to early Miocene, differences in deposition on the different margins of the Troodos remained (figure 3). Depositional environments in the south and east of the Troodos have been interpreted as shallow seas and lagoons, in the north as unrestricted carbonate-depositing seas and in the north-west the margins were subaerially exposed (Robertson, 1977). The northwestern margins therefore experienced erosion of facies but also the formation of reefs (Robertson, 1977). The north-western parts of the upper Lefkara unit thus show first signs of regional uplift towards the lower Miocene.

Miocene

The deep-sea pelagic carbonates of the Lefkara formation are replaced by the Pakhna formation in the early Miocene, which contains varied, shelf-depth carbonates and clastics (Kinnaird & Robertson, 2013). More specifically, the Pakhna formation contains both pelagic and hemipelagic carbonates, calciturbidites and mass-flow deposits (Kinnaird & Robertson, 2013). The depositional environments shallowed upwards from shallow seas to lagoons and localized reefs (Robertson, 1977). Uplift of the Troodos ophiolite has been inferred to have started in the Miocene. From apatite (U/Th)/He dating, an onset of uplift of 6 ± 2 Ma has been inferred (Morag et al., 2016). This timing is supported by the appearance of ophiolite-derived clasts in Miocene to early Pliocene conglomerates found in strata with an age of 5.5 million years (McCallum, 1989; Rouchy et al., 2001). In addition to that, deposition of Troodos-derived clasts seemed to have been simultaneous in both the Mesaoria and Pissouri basin (figure 2), indicating that the Troodos massif was uplifted as a single, coherent, tectonic unit (Kinnaird et al., 2011). Eventually, by the middle Miocene, the Troodos Massif was uplifted sufficiently to be subaerially exposed (Robertson, 1977). Uplift continued, with the centre of uplift in the Limassol Forest area (Robertson, 1977). However, to the north of the Troodos, the Mesaoria half-graben basin was actively subsiding, and this subsidence continued well into the Pliocene (McCallum & Robertson, 1995). Subsidence in the Mesaoria basin was caused by normal faulting, possibly due to the emplacement of the Kyrenia range (McCallum & Robertson, 1995; Robertson, 1977). During the rest of the Miocene, both uplift and subsidence continued contemporaneously, with subsidence taking place on the northern margin of the Troodos and uplift on the southern margin. This resulted in different types of sedimentation on the different margins of the Troodos: 1) the Limassol forest experienced partial erosion of (pre-) Miocene sediments due to its rapid uplift; 2) southeast of the Troodos, shallow water clastics and carbonates were deposited in an unstable basin; 3) in the Mesaoria basin to the north, deposition took place in shallow seas and 4) south of the Troodos, thick carbonate sediments were deposited in an actively subsiding basin (Robertson,

1977). Deposition of the Pahkna formation ended when the Kalavasos gypsum facies were deposited in the Messinian (Harrison et al., 2013).

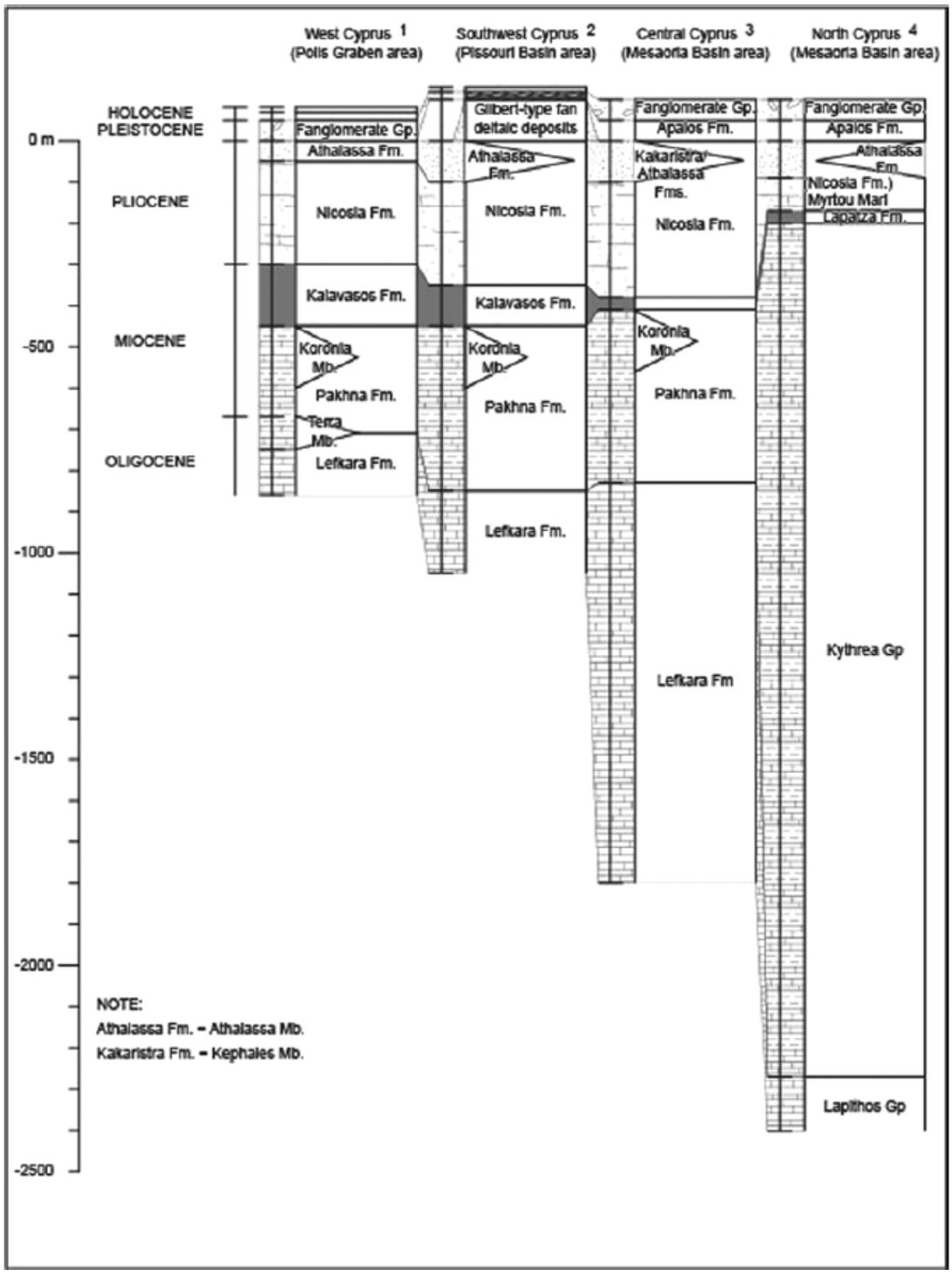

Figure 3 - Summarized stratigraphic column of Circum-Troodos sediments showing differences in thicknesses between the formations in different areas of Cyprus. In stratigraphic log 4, often the Turkish names for the stratigraphical formations are used. After: (Kinnaird & Robertson, 2013).

Pliocene

The Pliocene started with deposition of the Nicosia formation after marine transgression in the north (McCallum & Robertson, 1995; Robertson, 1977). A mature erosion face can be found at the Miocene-Pliocene boundary along the Akamas Peninsula (Poole & Robertson, 1991). Pliocene deposition consisted of a variety of shallow marine sediments, as basins in the north and east of Troodos were subsiding due to fault activity and basins in the south either were subaerial, thus experiencing deposition of coarse, Troodos-derived clastics or, if submerged, deposition of shallow marine sands and marls (Robertson, 1977). The marine siltstones are cut by conglomerate and sand-stone filled channels, which both fine upwards and distally (McCallum & Robertson, 1995). The subaerial and coastal parts of the Nicosia formation are no longer preserved (McCallum & Robertson, 1995). After deposition of the Nicosia formation, the shallow-marine Kakkaristra formation and the fluvial Apalos formation were deposited (figure 3, McCallum, 1989; McCallum & Robertson, 1995).

In the Mesaoria basin, both the Nicosia formation and the Kakkaristra formation consist of conglomerates containing Troodos-derived clasts, which thus preserve records of the uplift and unroofing of the Troodos massif (McCallum & Robertson, 1995; Poole & Robertson, 1991, 1998; Robertson, 1977). The oldest fan deltas in the Nicosia formation are of early Pliocene age and are exposed near the northern margin of the Troodos (Kinnaird et al., 2011). The deposition of these small, isolated fan deltas is inferred to have happened when the basin was subsiding, as the fan deltas seem to be fault-controlled (McCallum & Robertson, 1995). The outward progradation of these fan deltas documents continuing uplift and erosion of the Troodos mountains (McCallum & Robertson, 1995). The fans of the Nicosia formation are single, isolated units that never formed a large fan structure, possible restricted by the fault-block morphology in the Mesaoria basin (McCallum & Robertson, 1995). The younger fan deltas of the Kakkaristra formation have been deposited when subsidence had stopped and the Mesaoria seaway had been filled with sandy sediment, forming a shallow sea (McCallum & Robertson, 1995). The Kakkaristra formation lies partially unconformable on the Nicosia formation (McCallum & Robertson, 1995). Depositonal environment of the Kakkaristra formation has been interpreted to have been deltaic, as it contains wave- and stream-affected facies (McCallum & Robertson, 1995). The Kephales Member of the Kakkaristra formation, the member containing the conglomeratic deposits, has been dated between 2.58 and 1.95 Ma, and thus documents a second phase of fan delta deposition (Kinnaird et al., 2011).

Pleistocene

Uplift of the Troodos continued well into the Pleistocene, as the Pleistocene Fanglomerate deposits mark a transition from marine to non-marine sediments (Kinnaird et al., 2011). Uplift rates have been estimated to have peaked during the early to middle Pleistocene (Poole & Robertson, 1998). The oldest Pleistocene sedimentary unit contains conglomerates that have been deposited by an alluvial fan, and has thus been named the Fanglomerate group (Poole & Robertson, 1991, 1998). The Fanglomerate group mostly unconformably overlies the Pliocene units and locally makes incisions into the Troodos massif (Poole & Robertson, 1991). The fan deposits contain coarse, immature and poorly sorted sediment that has been interpreted to have been released by pulses of large uplift (Robertson, 1977). The largest difference between the Pliocene and Pleistocene conglomerates is that the Pleistocene conglomerates contain a greater percentage of diabase and gabbro clasts, in addition to the clasts generally being more fine-grained (Poole & Robertson, 1991, 1998). Almost no pelagic-derived clasts are found in the younger fans, as diabase is more erosionally resistant and most of the eroded carbonates had been disaggregated by then (Poole & Robertson, 1998). The youngest fanglomerates have been dated at 185-219 ka and 116-134 ka (Poole & Robertson, 1998). Uplift has been inferred to have continued after 0.78 Ma, as the

youngest marine terraces that have been covered with littoral sediments are of that age (Kinnaird et al., 2011).

1.3 Serpentinization

General

Serpentinites are rocks that mostly consist of the minerals from the serpentinite group (antigorite, lizardite, chrysotile) and magnetite and brucite (Guillot et al., 2015). They form during the process of serpentinization, which is a hydration reaction occurring in ultramafic material at temperatures between 100^0 and 700^0 Celsius (Guillot et al., 2015). The general structural formula of the minerals of the serpentine-group is $Mg_3Si_2O_5(OH)_4$ (Guillot et al., 2015). Al^{3+} is common at higher temperatures to provide more stability, whereas a substitution of Fe^{3+} is common at low temperatures in hydrothermal environments (Guillot et al., 2015a). The general reaction is:

Olivine + enstatite + H_2O = serpentine + magnetite (+ H_2) (Guillot et al., 2015).

Common secondary minerals are talc, calcite and magnesite (Guillot et al., 2015).

Varieties

Lizardite and chrysotile are stable at low pressure ($P < 1.0$ GPa)/low temperature conditions, whereas antigorite is the high P/high T variety (Guillot et al., 2015). Of the two low P/low T varieties, lizardite forms first, especially if the water:rock ratio is low (Andreani et al., 2007). When water:rock ratio is high, chrysotile forms (Andreani et al., 2007). The change from lizardite to antigorite starts at a temperature of 320^0C and is completed at a temperature of 390^0C (Guillot et al., 2015). In general, serpentine minerals are stable in a large variety of P/T conditions and environments (Guillot et al., 2015).

The reaction on microscale

Serpentine reactions make use of the microfractures that extend along multiple grains of olivine and enstatite that are often already present in a rock due to thermal and tectonic stresses (Rouméjon & Cannat, 2014). The reaction is initiated along two microfractures that intersect at angles of 55^0, which creates the typical serpentine mesh rims (Rouméjon & Cannat, 2014). During serpentinization and subsequent volume increase, the rock starts to fracture more (Rouméjon & Cannat, 2014). These smaller, perpendicular microfractures can now be used as pathways for fluids to enter the rock (Rouméjon & Cannat, 2014). The mesh rims form when fluid:rock ratio is low, but fluid must be available for the reaction to occur (Rouméjon & Cannat, 2014). As the serpentinization degree of a rock increases and water:rock ratio is high, the olivine in the mesh cores is replaced by isotropic serpentine (Rouméjon & Cannat, 2014). An extensive degree of serpentinization of 70-80% with a mesh texture of between 30 and 140 micrometers is able to form in the lab within 1100 days if fluid supply is sufficient, which is geologically instantaneous (Rouméjon & Cannat, 2014). However, the time it takes for active serpentinization outside the lab can be highly variable, due to fluid availability, fluid circulation and permeability (Rouméjon & Cannat, 2014).

Geological setting

For the process of serpentinization to occur, fluids must be able to get into contact with the ultramafic rocks of the oceanic lithosphere. This can happen in a multitude of environments. Water can enter the lithosphere in or near mid-ocean ridge environments through (transform) faults (Prichard, 1979). In a subduction zone, serpentinization can happen as water becomes available through slab dehydration, which will serpentinize the overlying mantle wedge (Guillot et al., 2015). After exhumation and exposure of ultramafic mantle material, as often happens in ophiolites, meteoric water can also infiltrate the rock (Magaritz & Taylor, 1974).

Implications for rheology

The process of serpentinization has important implications for the rheology of the lithosphere. Lizardite and chrysotile have a low friction coefficient and low fracture strength (Escartín et al., 2001). The strength of serpentinized peridotite reduces to the strength of pure serpentinite when the degree of serpentinization exceeds 15% (Escartín et al., 2001). In addition to a low friction coefficient and low fracture strength, serpentine minerals have low densities. During serpentinization, the bulk density of the rock decreases from 3300 kg m^{-3} to 2600 kg m^{-3} (Schuiling, 2011). During the process, volume can increase up to 40% (Guillot et al., 2015; Schuiling, 2011). Due to its low density and thus high buoyancy, serpentinite diapirism has been one of the proposed mechanisms for creating the topography now observed on the island of Cyprus (e.g., Schuiling, 2011).

Cyprus

On the island of Cyprus, serpentinite can be found in three areas: in the Mamonia Complex, the Limassol Forest and in the centre of the Troodos (figure 2). The serpentinites of the Troodos have high oxygen and hydrogen isotopic signatures that indicate serpentinization through low temperature, meteoric or oceanic fluids (Magaritz & Taylor, 1974; Nuriel et al., 2009). No consensus on timing of serpentinization has been reached, as the serpentinite has been interpreted to be of both Cretaceous (Nuriel et al., 2009; Schuiling, 2011) and Miocene age (Magaritz & Taylor, 1974). Multiple studies find different chemical signatures in the partly serpentinized area and the fully serpentinized area of the Troodos mountains. For example, Evans et al. (2021) finds that the two domains have different bulk densities and stable oxygen and hydrogen isotope values. They have interpreted this as a result of differential serpentinization.

2. Methods

2.1 Acquisition of field data

2.1.1 Method of data collection

Fieldwork is conducted to unravel the recent uplift phases and rates, by studying 24 fan deposits from the Miocene or younger. First, it is necessary to gain good understanding of each of the different lithological ophiolitic and sedimentary formations present in the Troodos mountains, so that the provenance of the clasts in the fan deposits could be recognized and determined. In the ophiolite and overlying sediments, distinguishing factors such as mineral content, grain size, presence of amygdales and vesicules are identified of the different formations before studying the clasts in the fans. The conglomerates in the fan deposits are of different generations and belong to the Pahkna Fm (Miocene), Nicosia Fm (Pliocene), Kakkaristra Fm (Pliocene-Pleistocene) and the Fanglomerates (Pleistocene) (see section 1.2.3 for detailed information on these specific formations). The sediments are studied with a major focus on clast content and clast characteristics and a minor focus on fossil content, matrix or cement composition, the angle of deposition and the orientation of the clasts. Facies descriptions are made of each of the 24 fan deposits. For eight fans, sedimentary logs are made to highlight the facies characteristics of each of these fans. In each fan, a selection of the clasts larger than 2cm are studied to identify the provenance of those clasts. Then, I estimate what the proportion of the different ophiolitic lithologies and sedimentary formations was in the fan.

2.1.2 Method of data analysis

To calculate the uplift rates, the clast data is used to see which clasts are introduced during which formations. The emergence of a type of clast provides a time constraint of when the formation the clast belongs to must have started to erode. These timelines are then compared to the thickness of the Troodos ophiolite to calculate uplift rates.

2.1.3 Analysis of serpentinites

Four samples of either fully or partly serpentinized material are cut into thin sections and studied under the optical microscope and scanning electron microscope (SEM). Two of these samples are collected within the Mount Olympus domain and two samples were taken from the Arakapas fault zone in the south. When analysing the serpentinites, focus is on the mineralogy, the microstructures and the veins.

2.2 Numerical method

For the modelling part of this thesis, PAR(O)VOZ is used, which is a thermomechanical algorithm adapted from the Fast Langrangian Analysis of Continuum (FLAC, (Cundall, 1989)). It is a method that uses a combined finite element/finite difference approach and it includes particle-in-cell technique, which provides the opportunity to trace and interpolate variables during dynamic remeshing (Yamato et al., 2007). The algorithm solves both the Newtonian motion equations and the heat transfer equations in Langrangian formulation (Le Pourhiet et al., 2004). In the model, rheological behaviour is set to be visco-elasto-plastic and is determined by the combination of the temperature, state of stress and strain rate (Le Pourhiet et al., 2004; Yamato et al., 2007). For a more detailed description of the numerical method, the reader is referred to the literature (Burov, 2011; Le Pourhiet et al., 2004; Yamato et al., 2007, 2008).

2.3 Model set-up and boundary conditions

2.3.1 Initial geometry

The initial model box dimensions are 1000 km long by 660 km deep (figure 4). The spatial mesh resolution is 2.5x2.5km. The initial geometry consists of a subducting slab that is at approximately 100km depth in the initial state. The downgoing plate has an overall thickness of 50km, which includes a 7.5km thick oceanic crust. The overriding plate in the reference model is 30km thick, with a 7.5km thick oceanic crust as well. Throughout the parameter study, crustal thickness remains unchanged, which is slightly thicker than the average oceanic crust, which was needed for model stability. The slab dip is either 15 degrees (shallow) or 30 degrees (steep). The choice for these two dip-values was made on published estimates, which range between 13 and 33 degrees (Feld et al., 2017; Mackenzie et al., 2006).

2.3.2 Initial geotherm

The temperature within the crust follows a linear gradient from 0^0C at the top to 500^0C at the Moho (table 1). In the lithosphere, it increases from 500^0C to 1330^0C at the lithosphere–asthenosphere boundary. In the mantle, the temperature increases up to 1400^0C at 660 km depth.

2.3.3 Boundary conditions

A horizontal velocity of 1 cm/yr is placed at both sides of the model. This convergence rate does not change during run time of the models. In addition to that, the convergence rate is the same for all models. The convergence rate of 1 cm/yr was chosen based upon present-day GPS data, in which the African plate moves towards a stationary Europa with approximately 2 cm/yr (Fernandes et al., 2003). However, the downgoing plate buckles when a convergence rate of 2 cm/yr is applied to it due to the lithospheric strength of the plate. Therefore, a horizontal velocity of 1cm/yr is applied to both sides of the model. As the oceanic crust is inferred to be of Turonian age (Blome & Irwin, 1985; Mukasa & Ludden, 1987) and the overlying Lefkara formation is of Maastrichtian age (Blome & Irwin, 1985; Robertson, 1977), the duration of the process of emplacement of the Troodos crust is interpreted to have taken 10myr. Therefore, the models are all run for 10myr.

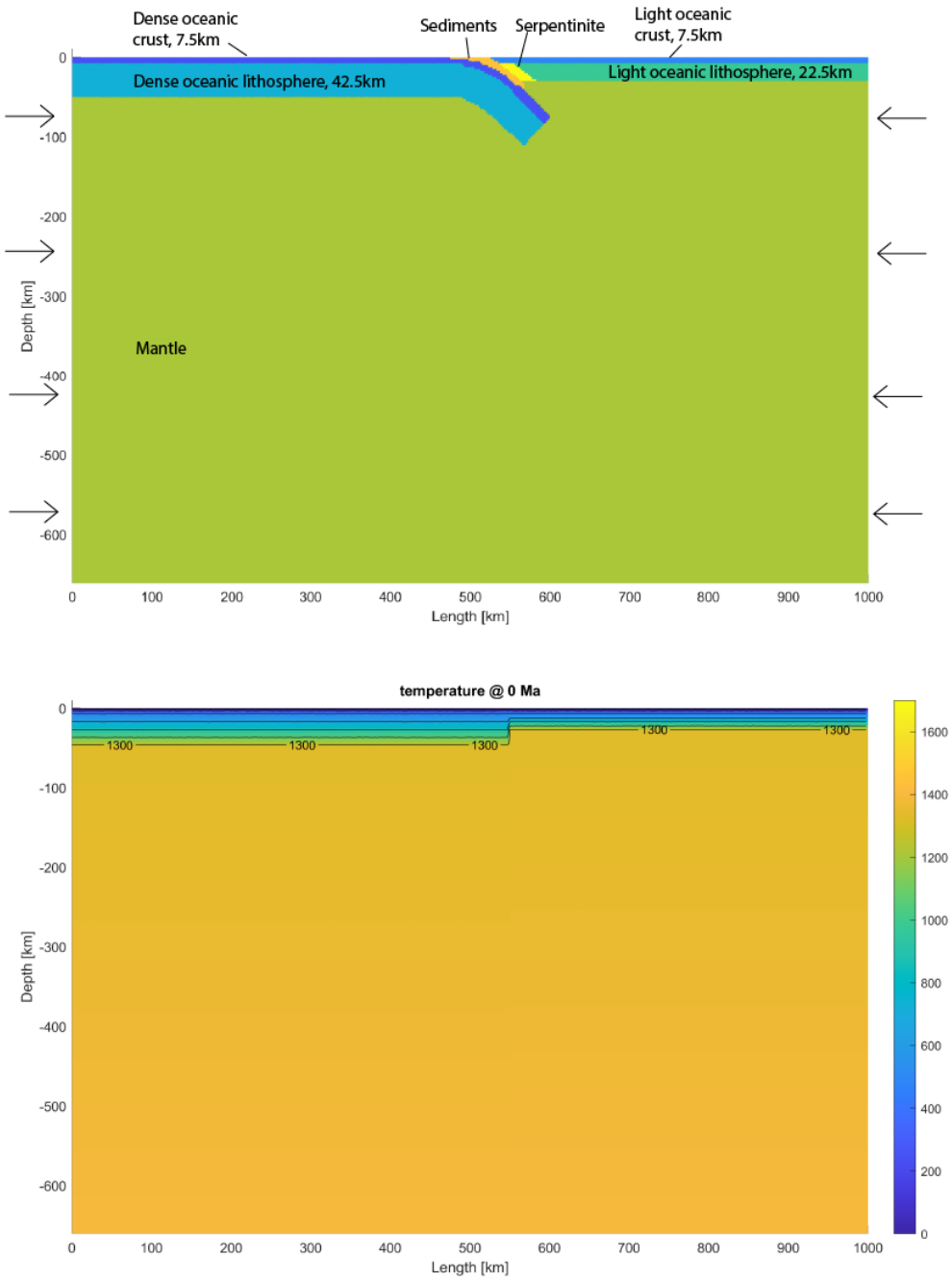

Figure 4 - Initial model box for a model with a steep slab showing the subduction zone at t = 0 Ma. The model box here shows a thick serpentinite wedge. The thickness of this wedge differs per model, but is shown here to demonstrate the position and shape of the serpentinite wedge.

2.3.4 Rheology parameters

Rheology parameters are obtained from literature (table 2, figure 5). These have been chosen based on a number of criteria: 1) the overriding plate had to be heavy enough to subduct, therefore there should be a small rheological difference between the downgoing and overriding plate; 2) strain should localise in the subduction zone; 3) the slab should remain attached to the plate and not 'drown' on its own, i.e. the slab has to be brittle. The first criterium is achieved by ensuring that the density of the overriding plate's crust and lithospheric mantle is larger than the densities of the downgoing plate.

The serpentinite densities used in the models are adapted from Evans et al. (2021). Most papers estimate the density of serpentinite to be approximately 2600 kg/m^3. Evans et al. (2021) has indeed measured a density of ~2600 kg/m^3 for the 50-70% serpentinized harzburgites. However, the 90-100% serpentinized rocks have densities of ~2300 kg/m^3 and ~1500 kg/m^3, resulting in a gross bulk density of ~1900 kg/m^3. Therefore, the bulk density of ~1900 kg/m^3 is taken as a lower limit, even though it might be considered lower than what is usually considered as a normal value for the bulk density of serpentinite. A value of 2300 kg/m^3 is taken as an in-between value. This is done to ensure that we have a wider range of serpentinites to model with and that these values are appropriate for the Troodos serpentinites.

The thickness of the different layers needs to be 3px, i.e. 7.5km, at least for the model to be able to work. Therefore, the sediment layers, the oceanic crust and the thin serpentinite layers are all 7.5km thick minimum.

2.3.1 Model parameters and parameter sensitivity of boundary conditions

A parametric study (model 1-12) is performed, in which the influence of the following parameters on the resulting topography is tested: 1) the lithospheric thickness of the overriding plate; 2) the rheology of the material that is situated in between the two plates which enables movement between the two during modelling (table 3). The models are analysed with regards to maximum elevation, uplift rates, elevation across the topographic profile (in km) after 10 Ma and geometry (table 3). The geotherm changes according to the lithospheric thickness that is used.

2.3.5.1 Lithosphere thickness of the overriding plate

Shallow slab (15 degrees dip angle)

For models with a shallow subduction angle, maximum elevation of the models ranges between 6-7km for lithosphere thicknesses of 30 km to 40 km (table 3). Final elevation ranges from 3-3.5km. The thickness of the overriding plate's lithosphere has marginal effect on both maximum elevation and the final elevation for models with a shallow slab. The uplift rates in all models are stable at 0.3 cm/yr. Model 2 is used as a reference model for the shallow slab models in the main model set (models 15-38).

Table 1 - Thermal parameters used in the model. The parameters are based on literature or considered standard values.

Thermal parameters	*Thermal property*	*Value*	*Unit*	*Reference*
	Surface temperature	10	^{0}C	
	Temperature at the base of crust	500	^{0}C	
	Temperature at the base of lithosphere	1330	^{0}C	
	Thermal conductivity crust	2.5	W/m ^{0}C	
	Thermal conductivity mantle	3.5	W/m ^{0}C	
	Radiogenic heat production at surface	1.5e-9	W/kg	
	Radius radiogenic heat	10	km	
	Thermo-tectonic age of lithosphere	2	Myr	(Mukasa & Ludden, 1987)
	Surface heat flow	40	mW/m^2	
	Mantle heat flow	15	mW/m^2	

Table 2 - Mechanical parameters used in models. The viscosity parameters are based on literature. The density is varied, to create a dense subducting and light overriding plate. 1:(Caristan, 1980) ; 2: (Mackwell et al., 1998) ; 3:(Karato et al., 1986) ; 4: (Goetze & Evans, 1979); 5:(Evans et al., 2021) ; 6: random

Mechanical parameters	*Mechanical property*	*Value*	*Unit*
Dense upper crust *Basalt* [1]	Density	3200	kg/m^3
	Viscosity parameter N	3	
	Viscosity parameter A	6.3e-2	$MPa^{-n}\ s^{-1}$
	Viscosity parameter E	2.76e+5	J/mol
Light upper crust *Basalt* [2]	Density	3100	kg/m^3
	Viscosity parameter N	4.7	
	Viscosity parameter A	1.9e+2	$MPa^{-n}\ s^{-1}$
	Viscosity parameter E	4.85e+5	J/mol
Dense lithospheric mantle *Dry olivine* [3]	Density	3330	kg/m^3
	Viscosity parameter N	1	
	Viscosity parameter A	7.7e-9	$MPa^{-n}\ s^{-1}$
	Viscosity parameter E	5.36e+5	J/mol
Light lithospheric mantle *Dry olivine* [3]	Density	3200	kg/m^3
	Viscosity parameter N	1	
	Viscosity parameter A	7.7e-9	$MPa^{-n}\ s^{-1}$
	Viscosity parameter E	5.36e+5	J/mol
Asthenosphere *Wet olivine* [4]	Density	3250	kg/m^3
	Viscosity parameter N	3.0	
	Viscosity parameter A	7.0e+3	$MPa^{-n}\ s^{-1}$
	Viscosity parameter E	5.1e+5	J/mol
Serpentinite [2 5]	Density A/B/C	2600/2300/1900	kg/m^3
	Viscosity parameter N	4.7	
	Viscosity parameter A	1.9e+2	$MPa^{-n}\ s^{-1}$
	Viscosity parameter E	4.85e+5	J/mol
Sediment [6]	Density	2400	kg/m^3
	Viscosity parameter N	3.05	
	Viscosity parameter A	6.8e-6	$MPa^{-n}\ s^{-1}$
	Viscosity parameter E	2.76e+5	J/mol
	Friction angle	30^0	
	Lamé elastic constant	4e+10	N/mm^2
	Cohesion	20e+6	kPa
	Erosion coefficient (a)	500	m^2/yr

Steep slab (30 degrees dip angle)
The steep slab models show more variation in uplift rate and elevation after 10 Ma (table 3). Uplift rates vary between 0.2-0.5 cm/year and the elevation after 10 Ma ranges between 1.5 km for thin lithospheres and 4 km for thick lithospheres. The maximum elevation is identical for the models with 30-40 km thicknesses: it ranges between 5.5 and 6km, in which the thicker 40km plate results in a maximum elevation of 6km. Geometries of the topographic profiles for both sets of models are either sinusoidal or irregular. Model 1 is used as a reference model for the steep slab models in the main model set (models 15-38).

For the main model sets (model 15 to 38, including M1_e and M2_e), the lithosphere has a 30km thick lithosphere for the overriding plate. This value was chosen because the shallow slab models show very little variation in uplift rate and maximum elevation and the models are therefore considered numerically stable. The steep slab models show larger variation in uplift rate and elevation after 10 Ma. The 30km thick model has the lowest values for maximum elevation and elevation after 10 Ma, and therefore, a 30km thick lithosphere was chosen, as it leaves sufficient room to focus on the uplift created by serpentine.

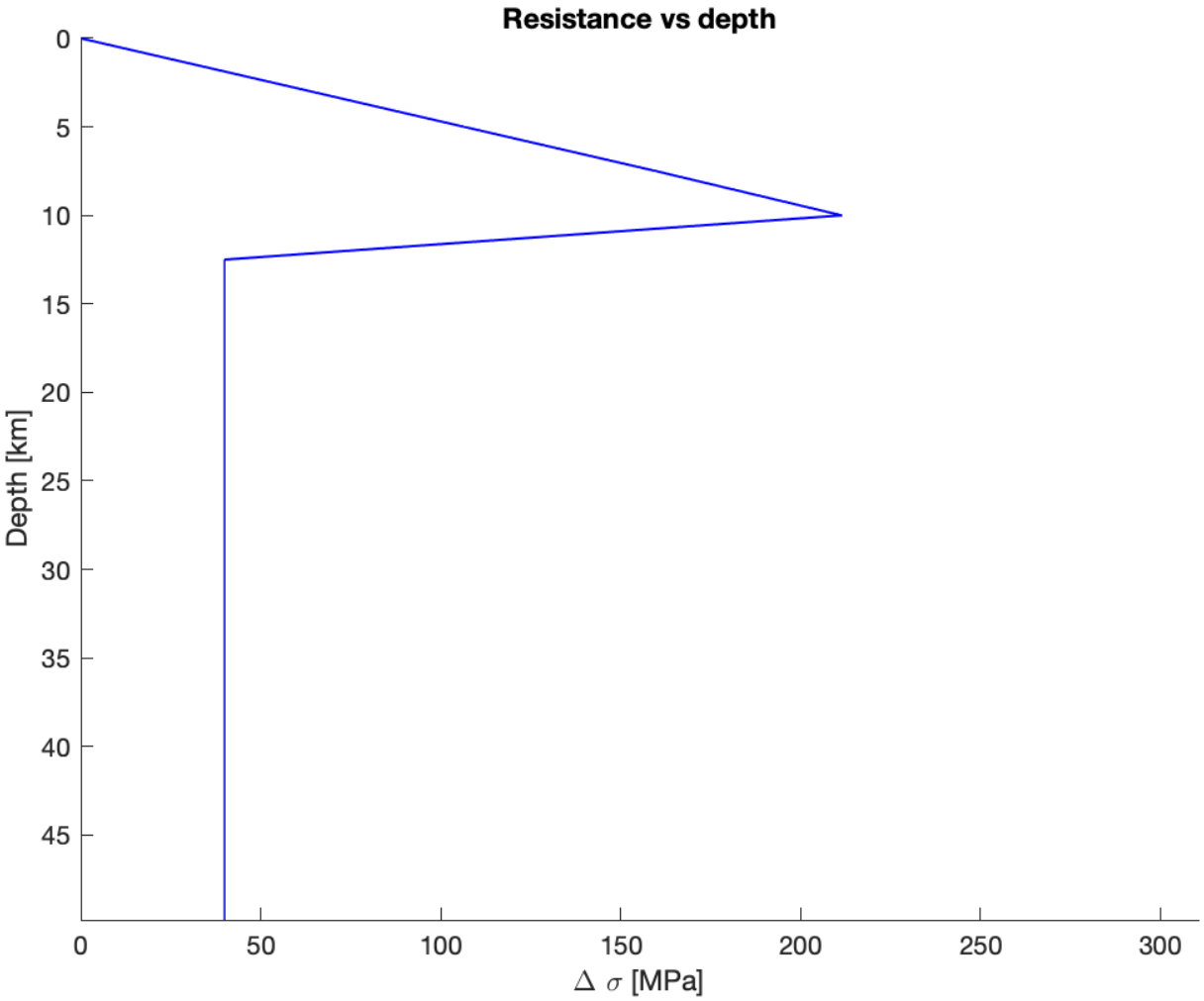

Figure 5 - graph showing rheology of subducting plate. Subducting plate is made of oceanic material. The rheology parameters of the overriding plate, except that it is slightly denser and 30km thick instead of 50km as the subducting plate is.

Table 3 - Parameters and results of parameter sensitivity test. Subd. Angle = subduction angle; litho = lithosphere; serp = serpentinite; sed = sediment.

Parameters						*Results*					
Model name	Subd. angle	Litho thickness	Thickness serp	Plate interface	Erosion	Max elevation in km	Timing to create peak in Ma	Uplift rate (km/Ma)	Uplift rate (cm/yr)	Final uplift	Shape
1	30	30	0	Sed	No	5	2	2.5	0,3	3	Sinusoidal
2	15	30	0	Sed	No	6	3	2	0,2	3	Irregular
3	30	35	0	Sed	No	5	2	2.5	0,3	3.3	Sinusoidal
4	30	40	0	Sed	No	5.5	2	2.8	0,3	3	Sinusoidal
5	15	35	0	Sed	No	7	3	2.3	0,2	3.3	2 peaks
6	15	40	0	Sed	No	6.5	2	3.3	0,3	4.1	2 peaks
7	30	30	0	Serp	No	5	1	5	0,5	1.5	Irregular
8	15	30	0	Serp	No	7	3	2.3	0,2	4	Sinusoidal
9	30	35	0	Serp	No	5	2	2.5	0,3	4	Sinusoidal
10	30	40	0	Serp	No	4.5	2	2.3	0,2	4.3	Sinusoidal
11	15	35	0	Serp	No	6.3	3	2.1	0,2	3.5	Sinusoidal
12	15	40	0	Serp	No	8	7	1.1	0,1	6.3	Irregular

2.3.5.2 Plate interface material

Another boundary condition test was done to identify the effect of various types of plate interface materials on the model efficiency and the resulting topography. Six models (models 7-12, table 3) were run to test serpentinite as the plate interface material instead of sediment. This caused a larger variety in maximum elevation (ranging from 4.5-8km with serpentine compared to 5-7 with sediment); a larger variation in time it takes to produce maximum elevation (from 1-7 Ma vs. 2-3 Ma) and larger variety in elevation after 10 Ma (1-6.25 km vs. 3-4km). Therefore, the choice was made to continue the rest of the models using sediment as the plate interface material, as these models seem to be more numerically stable and show less variation in maximum elevation, and uplift rates. Numerical stability and less variation is desired, as a numerical stable model provides a good baseline measurement, so that the influence of the serpentinite can be studied well.

After analysis of the parameters, 26 models are run in which the following parameters are varied: 1) the thickness of the serpentinized mantle lithosphere; 2) the density of the serpentinite; 3) erosion. This is done in order to be able to analyse what the influence of serpentinite is on the topography. All other parameters remain equal to the ones used in the reference models (model 1 and 2).

3. Results

3.1 Field data

3.1.1 Overview ophiolite section

To recognize the clasts in the fans in the field, the ophiolite sequence was studied. Diagnostic criteria of each section were described so that the rocks could be recognized later. The description of the rocks is found here below, starting with the stratigraphically deepest rocks.

Mantle

The mantle sequence consists of serpentinites and harzburgites. The serpentinites are very fibrous and have a white-greenish colour. Chrysotile is very abundant and has a silky lustre. Antigorite is glassy green and associated with magnesite, which is whitish and looks 'dusty'. The harzburgites have a brown rust colour, with larger, shining pyroxene crystals, showing two clear cleavage planes.

Crust

The crustal part of the ophiolite sequence starts with dunite and chromite at the bottom. The dunite contains over 90% weathered olivine and 10% (or less) olivine. Because of the weathering, the rock looks yellowish/ochre. The chromite is black and very fine grained.

The gabbros can be found either as layered gabbros or as massive gabbros. They contain plagioclase and pyroxenes. The layered gabbros have alternating pyroxene and plagioclase-rich layers. Crystals are 1-3mm large. The massive gabbros contain pegmatitic veins, in which the veins also have gabbroic composition. In these gabbros, green amphiboles can be found in addition to the plagioclase and pyroxenes. Grain size varies throughout the gabbros; from 1-15 mm.

The plagiogranites are generally found at the base of the sheeted dyke complex. They contain large amounts of plagioclase, in addition to quartz and hornblende. The hornblende crystals are very elongated, black and needle-like. Generally speaking, the plagiogranites are finer grained than the gabbros.

The sheeted-dyke complex contains dolerite or micro-gabbro (called diabase in literature). The rock is very fine-grained and weathers dark greyish with a slight blue-green hue. The dykes show

chilled margins. The rocks are massive, in the sense that they do not contain vesicules or amygdales.

The pillow basalts and the basal group contain very fine-grained basalts, so mineralogy-wise they are very similar to the sheeted-dyke complex. The presence of amygdales filled with quartz, calcite and zeolite and vesicules within the pillow basalts can help to distinguish these rocks from the group described above.

The umbers often have bright, vivid colours such as red, ochre, yellow, deep black or brown. The rock itself looks very massive, as it is extremely fine-grained: except for some secondary minerals, no crystals can be seen with the naked eye. They contain quartz and oxidized minerals, such as (chalco-)pyrite. Sometimes, these minerals grow inside veins in the rock.

Sediments
The limestones of the Lefkara formation are whitish to slightly pinkish in colour. They contain thin beds, 2-20cm thick, consisting mostly of wackestones with radiolarians. The grain size is fine silt. The bioturbation consists of single burrows, which are unlined and unbranched.

The limestones of the Pakhna formation are highly fossiliferous. The matrix is made of ochre yellow coarse silt. Most of the limestones are packstones, but some are wackestones. They contain shell fragments, intact bivalves, foraminifera, corals and gastropods.

3.1.2 Description of fans

Pakhna fans
The Pakhna submarine fans are the only monomict fans that have been studied (figure 6). They are poorly to very poorly sorted, with clasts ranging from a few mm to over 2m. Clasts are often still very angular. All clasts in the Pakhna submarine fans are from the Pakhna formation itself.

Nicosia fans
The Nicosia fans are very poorly to moderately sorted, with clasts ranging from 0.5mm to over 1m in some fans (figure 6 and 7). Clasts are angular to subrounded. Nicosia fans contain at least 20% to over 50% of limestone clasts from the Pahkna and Lefkara formations. The next major lithological group is the pillow basalts, comprising 10-60% of the clasts. The Nicosia fans do contain clasts from the sheeted dyke complex, but most Nicosia fans have more pillow basalt clasts than microgabbro clasts. No plagiogranite is encountered in these fans. Only one of the Nicosia fans contains gabbroic clasts. Also, the umber group is not very prevalent in these fans.

Fans 2.3a and 2.3b are from the same outcrop (figure 7), in which 2.3a is the younger fan. These fans show that within the time of deposition of the Nicosia formation, the clast content of the fans become more diverse: during this time, microgabbro becomes more prevalent and gabbros are eroded and deposited for the first time as clasts.

Kakkaristra fans
The Kakkaristra fans are all very poorly sorted, except for one (figure 6 and 8). Clast sizes go up to 50cm and are subangular to rounded. The Kakkaristra fans show high variability in clast content, but all lack limestone clasts. Umbers make up only 1-5% of clast content but are found in all fans. Pillow basalt clasts are between 10-20% of clast content in most of the fans, except for two, in

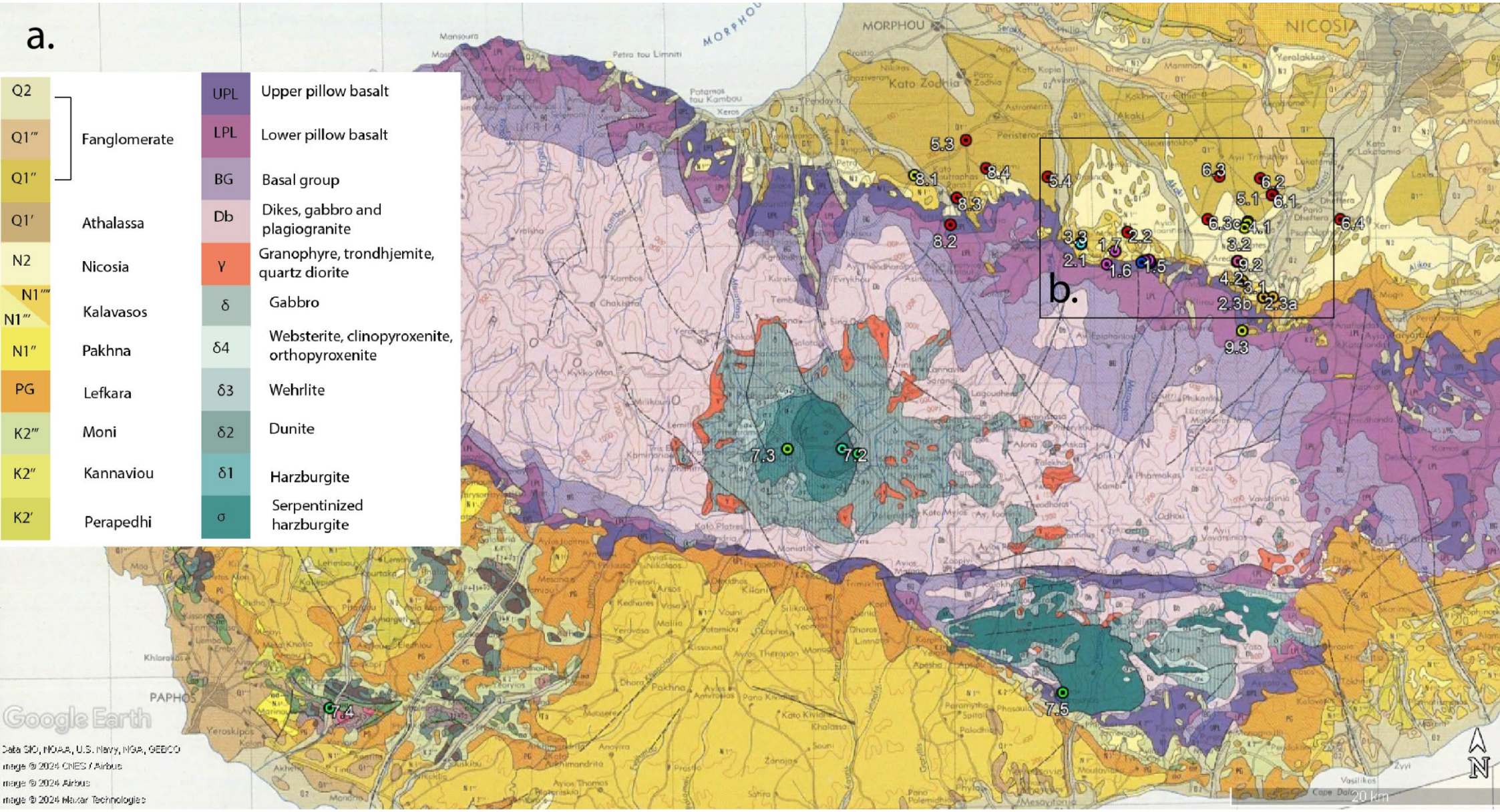
a.
Q2
Q1‴
Q1″
Q1′
N2
N1⁗
N1‴
N1″
PG
K2‴
K2″
K2′
Fanglomerate
Athalassa
Nicosia
Kalavasos
Pakhna
Lefkara
Moni
Kannaviou
Perapedhi
UPL
Upper pillow basalt
LPL
Lower pillow basalt
BG
Basal group
Db
Dikes, gabbro and plagiogranite
γ
Granophyre, trondhjemite, quartz diorite
δ
Gabbro
δ4
Websterite, clinopyroxenite, orthopyroxenite
δ3
Wehrlite
δ2
Dunite
δ1
Harzburgite
σ
Serpentinized harzburgite
b.
MORPHOU
NICOSIA
PAPHOS
Google Earth
20 km
N

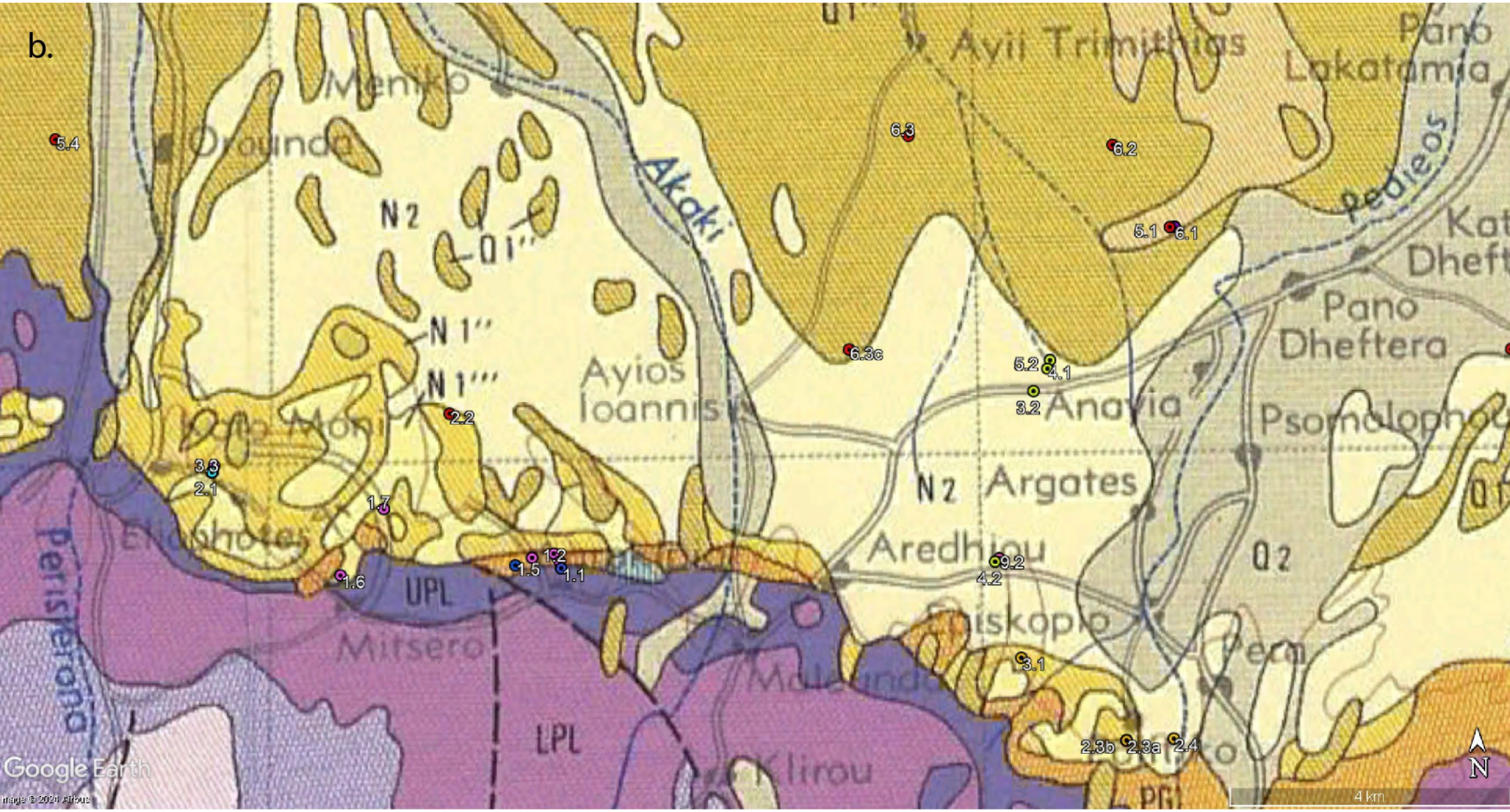
b.
Ayii Trimithias
Pano Lakatamia
Akaki
Pedieos
Pano Dheftera
Ayios Ioannis
Anovia
Argates
Aredhiou
Mitsero
Klirou
UPL
LPL
N2
O1''
N1''
N1'''
O2
5.4
6.3
6.2
5.1
6.1
6.3c
5.2
4.1
3.2
2.2
3.3
2.1
1.7
1.6
1.5
1.2
1.1
9.2
4.2
3.1
2.3b
2.3a
2.4
Google Earth
4 km
N

Figure 6 - a. Overview map of all field stops; b. Detailed section showing circum-Troodos sediment field stops. Geological base map is adapted from the European Soil Data Centre (Geological Map of Cyprus. - ESDAC - European Commission, n.d.).

which they make up 40 and 64% of clast content. The most prevalent clasts are those from the sheeted dyke complex, with the microgabbros making up 60-80% of clast content. Only in two fans was the microgabbro content much lower, in those it was 14 and 20%. Plagiogranites are found in 5 out of 7 fans, with percentages ranging from 1-20%. Gabbroic clasts are present in each of the fans, with percentages between 2-45%.

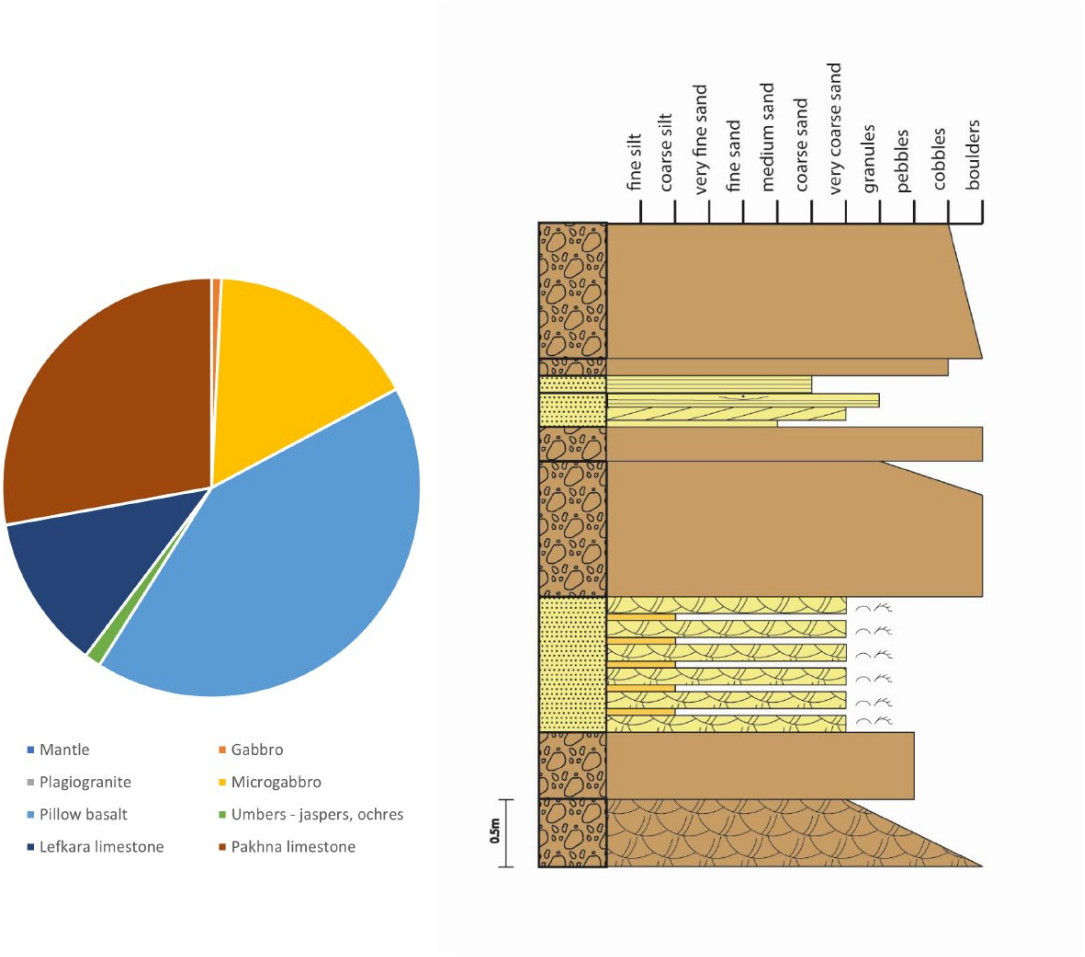

Figure 7 - Left: pie diagram of the average composition of the Nicosia formation fans. Right: sedimentary log of fans 2.3a and 2.3b, both belonging to the Nicosia Fm. The oldest fan 2.3b is the conglomeratic interval at the bottom. Fan 2.3a is found on top of the sandy intervals.

Fanglomerates

The fans of the Fanglomerates are very poorly to moderately well sorted. In most fans, the most abundant group are the microgabbros, with percentages ranging from 37-80% (figure 6 and 9). In contrast to the Kakkaristra, the Fanglomerates do sometimes contain limestone clasts, either from the Pakhna or the Lefkara formation. The limestone content is not more than 8%. Most of the fans contain umber clasts, with percentages ranging between 2-10%. Only two of them do not contain any umber. Generally, the ranges for the pillow basalts vary between 10-30%, except for fan 5.3, in which it is 40%. Plagiogranites can be found in most of the fans, with fractions between 2 and 20%. There is a lot of variation in the prevalence of the gabbros. In two fans, they are not present at all. In others, they make up 3-15% of the clast content. In three fans, olivine gabbro clasts were found.

3.2 Thermomechanical models

3.2.1 Evolution of representative models

The main core of the modelling exercises consists of 26 models that were run with varying values for density and thickness of serpentinite and variable subduction angles (table 4). Parameters and results can be found in table 4. Two large trends were shown.

In general, the shallow slab models had both higher maximum elevation of 6-14 km and final elevation of 3-11km, compared to 5.5-10.3km and 1-7km, respectively, for steep slab models (table 4). The shallow slab models reach their peak height in 3-9 million years. This leads to uplift rates of 0.1-0.3 cm/yr. The steep slab models reach their maximum elevation in the first three million years. Uplift rates are between 0.2-0.9 cm/yr. Two models that are representative for these two trends will be described next.

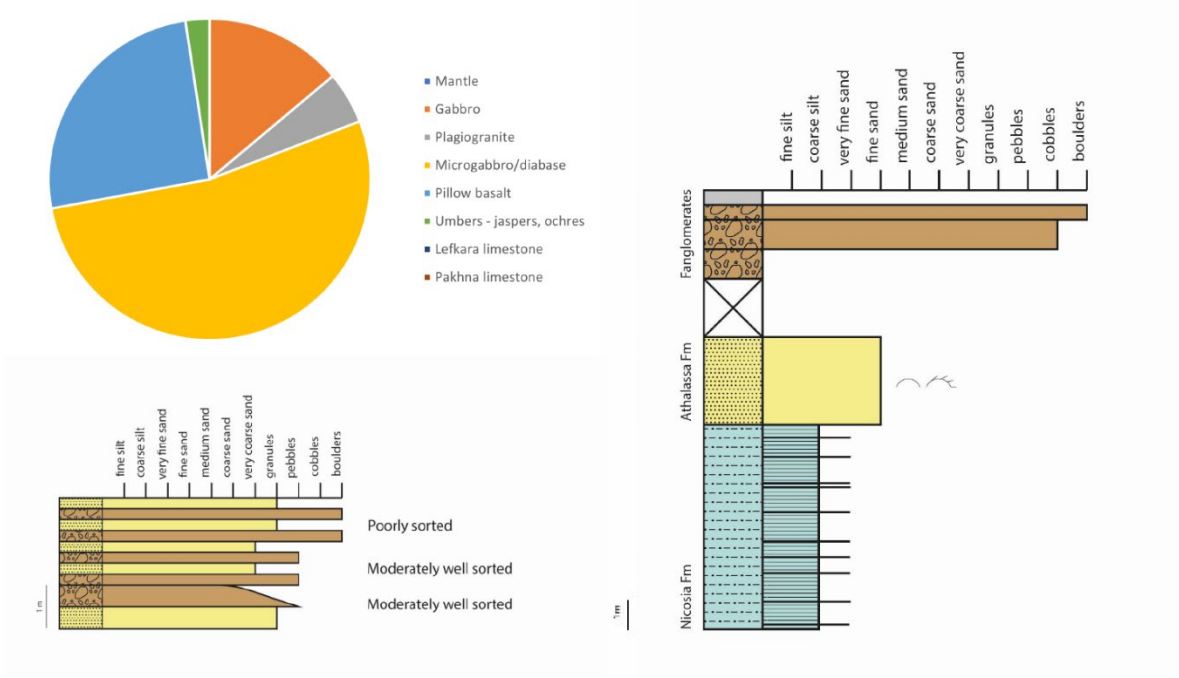

Figure 8 - top left: pie diagram showing the average composition of a Kakkaristra fans. Bottom left: sedimentary log of Kakkaristra fan, in which a regular change between more sandy and more conglomeratic intervals can be seen. Right: sedimentary logs showing the succession of the Nicosia, Athalassa and Fanglomerate formations, and the changes in facies observed in them.

Model 27

This model is representative for the steep slab models and is the erosive counterpart of model 15 (table 4, figure 10). During compression, the serpentinite moves towards shallower depths and becomes more tapered and wedge-shaped. Erosion starts after one million years. Within two million years, the maximum elevation of 6km is reached. The eroded material from the overriding plate ends up in the accretionary wedge after 3 Ma. The peak then subsides to 3km from 3-6 million years in model run time, after which elevation increases to slightly over 4km after 10 Ma. The uplift rate is 0.3cm/yr. The oceanic crust of the downgoing plate decouples as it enters the asthenosphere.

Model 34

This model is representative for the shallow slab models and is the erosive counterpart of model 22 (table 4, figure 11). The serpentinite forms a diapir and pierces into the overlying crust. This

process starts immediately in the first few million years. The model reaches its maximum elevation of 9.3 km after five million years, resulting in a low uplift rate of 0.2cm/yr. The topography shows two peaks, of which the highest is caused by the serpentinite and the lower is created by the accretionary wedge. The accretionary wedge in this model is much thinner than in model 27. After 10 Ma, the crust on the left side of the diapir is barely attached to the crust of the overlying plate on the right. The resulting topography is 8km high.

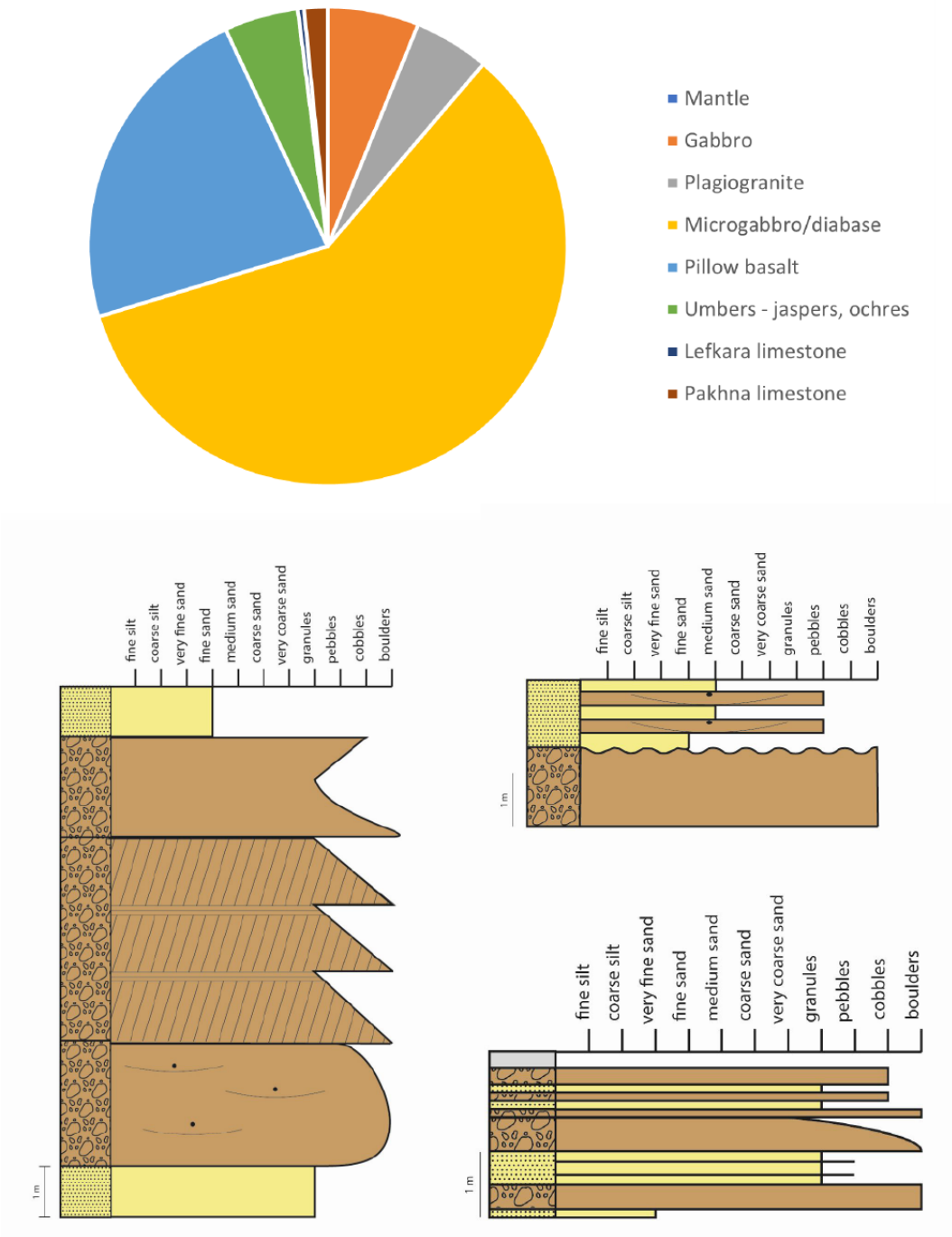

Figure 9 - Top: pie diagram showing average composition of the Fanglomerates. Bottom half: three sedimentary logs made of the Fanglomerate fans, showing the high diversity in clasts content and sedimentary structures found in the fans. Some fans are much larger than others, and some contain sandy intervals.

3.2.2 Comparison of model set

3.2.2.1 Thickness of serpentinized mantle lithosphere

Shallow slab models

For each of the shallow slab models with serpentinite, the trend shows that the thicker the serpentinite is, the larger the uplift is (i.e. 14km is the highest amount of uplift for a 12km thick serpentinite layer). The additional uplift of the serpentinite models compared to the reference model ranges within 1-8 km, with only one model (no. 20) that has an equal uplift of 6 km to the reference model. Uplift rates, however, are smaller for models with serpentinite than for the reference model without: uplift rates of the serpentinite models vary within 0.1-0.4 cm/yr, in which only one model (model 26) with an uplift rate of 0.4cm/yr has a higher uplift rate than the reference model (0.3 cm/yr). Final elevation after 10Ma ranges within 5.5-12.5km for models without erosion and within 3-11km for those with.

Steep slab models

The steep slab models show higher maximum elevation for models with serpentinite than for those without, but the differences are not as large as the shallow slab models: maximum elevation ranges within 6-9km for models with erosion (compared to 5km in the reference model without erosion. When looking at maximum elevation, the thicker the serpentinite layer, the higher the maximum uplift. There is a larger difference in uplift rates for the steep slab models compared to the reference model, as uplift rates range within 0.2-0.9 cm/yr for serpentinite models without erosion and between 0.3-0.8 cm/yr for models with erosion. For the steep slab models without, there is a positive correlation between serpentinite thickness and final elevation. This correlation is not found when erosion is applied to those models.

3.2.2.2 Density of serpentinite

Generally, less dense serpentinite creates higher elevation of 8-14 km compared to 6-8 km for denser serpentinites for both the steep and shallow slab sets of models. The uplift rates, however, vary more and do not show clear trends, as they range from 0.1-0.9 cm/yr. In both model sets, the uplift rates of the models with 2600 kg/m^3 densities are very close to each other, all between 0.2-0.3 cm/yr. Variability in uplift rates increases with decreasing density. For shallow slab models without erosion, the final elevation increases with decreasing density. This trend is not seen in the steep slab models without erosion: in these models, the models with a density of 1950 kg/m^3 show less final elevation than the models with a density of 2300 kg/m^3.

3.2.2.3 Erosion

Shallow slab models

The maximum elevation and uplift rates of the models with erosion compared to those without erosion are similar or slightly higher (with a maximum of 1km difference). Final elevation of the models is lower when erosion is applied, 3-11km compared to 6-13km.

Steep slab models

The maximum elevation is also higher in models with erosion than in those without. Usually, the uplift rate is also similar, except for model 37, in which the uplift rate is barely half of the reference model. There is a large variation in final elevation: half of the models that include erosion have higher final elevation (4.3-7km) than their counterparts without erosion (3.5-5 km), but some have drastically less final uplift. When comparing the models without serpentinite, the models with erosion have a higher final elevation (4.5 km compared to 1.5km) and have experienced less subsidence at the end of the model run time.

Table 4 - Parameters and results of the main model set. Thickness of serpentinite is shown in px. One pixel is one cell size, i.e. 2.5km. The serpentinite is thus 0, 7.5 or 15 km thick in diameter.

Parameters							*Results*					
Model name	Subd. angle	Litho thickness	Thickness serp in px	Density serp	Plate interface	Erosion	Peak elevation in km	Timing of peak in Ma	Uplift rate (km/Ma)	Uplift rate (cm/yr)	Final elevation in km	Shape
15	30	30	3	2600	Sed	No	6	2	3	0.3	4	Sinusoidal
16	15	30	3	2600	Sed	No	7	3	2.3	0.2	5.5	Two peaks
17	30	30	6	2600	Sed	No	6	2	3	0.3	3.5	Sinusoidal
18	15	30	6	2600	Sed	No	7.3	3	2.4	0.2	6	Two peaks
19	30	30	3	2300	Sed	No	6	3	2	0.2	4	Irregular
20	15	30	3	2300	Sed	No	6	3	2	0.2	6	Sinusoidal
21	30	30	6	2300	Sed	No	7.5	1	7.5	0.8	5	Irregular
22	15	30	6	2300	Sed	No	9	6	1.5	0.2	9	Two peaks
23	30	30	3	1950	Sed	No	7.8	2	3.9	0.4	6	Sinusoidal
24	15	30	3	1950	Sed	No	8.5	9	0.9	0.1	8	Sinusoidal
25	30	30	6	1950	Sed	No	9	1	9	0.9	7	Sinusoidal
26	15	30	6	1950	Sed	No	14	4	3.5	0.4	12.5	Sinusoidal
M1_e	30	30	0		Sed	Yes	5.5	2	2.8	0.3	4.5	Sinusoidal
M2_e	15	30	0		Sed	Yes	6.3	2	3.2	0.3	5	Sinusoidal
27	30	30	3	2600	Sed	Yes	6	2	3	0.3	4.3	Sinusoidal
28	15	30	3	2600	Sed	Yes	6	2	3	0.3	3	Two peaks
29	30	30	6	2600	Sed	Yes	6.5	3	2.2	0.2	1.5	Irregular
30	15	30	6	2600	Sed	Yes	8	5	1.6	0.2	6	Two peaks

Parameters							*Results*					
Model name	**Subd. angle**	**Litho thickness**	**Thickness serp in px**	**Density serp**	**Plate interface**	**Erosion**	**Peak elevation in km**	**Timing of peak in Ma**	**Uplift rate (km/Ma)**	**Uplift rate (cm/yr)**	**Final elevation in km**	**Shape**
31	30	30	3	2300	Sed	Yes	6.2	3	2.1	0.2	5.5	Sinusoidal
32	15	30	3	2300	Sed	Yes	7	5	1.4	0.1	5.3	Irregular
33	30	30	6	2300	Sed	Yes	8	1	8	0.8	6.8	Sinusoidal
34	15	30	6	2300	Sed	Yes	9.3	5	1.9	0.2	8	Two peaks
35	30	30	3	1950	Sed	Yes	7.8	2	3.9	0.4	5	Sinusoidal
36	15	30	3	1950	Sed	Yes	9	5	1.8	0.2	7	Sinusoidal
37	30	30	6	1950	Sed	Yes	10.3	2	5.2	0.5	1	Irregular
38	15	30	6	1950	Sed	Yes	14	5	2.8	0.3	11	Two peaks

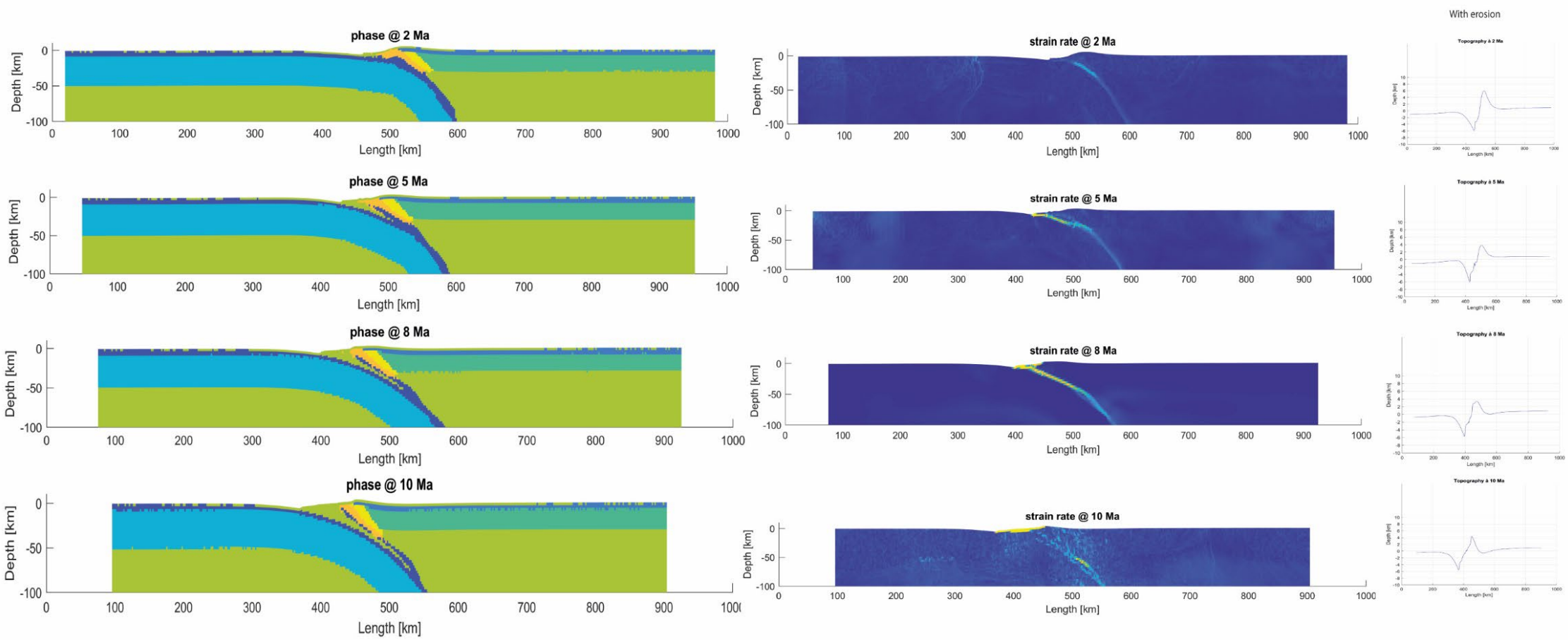

Figure 10 - summary of the model evolution of a typical steep slab model. The intervals shown are at 2, 5, 8 and 10 Ma. The model has an intermediate serpentinite wedge in thickness. The serpentinite ascends slightly. On the left of the serpentinite, an accretionary wedge forms, made up of sediments (orange) and erosional products (green). The strain can be seen to localize on the plate interface and on the accretionary wedge after 10 Ma.

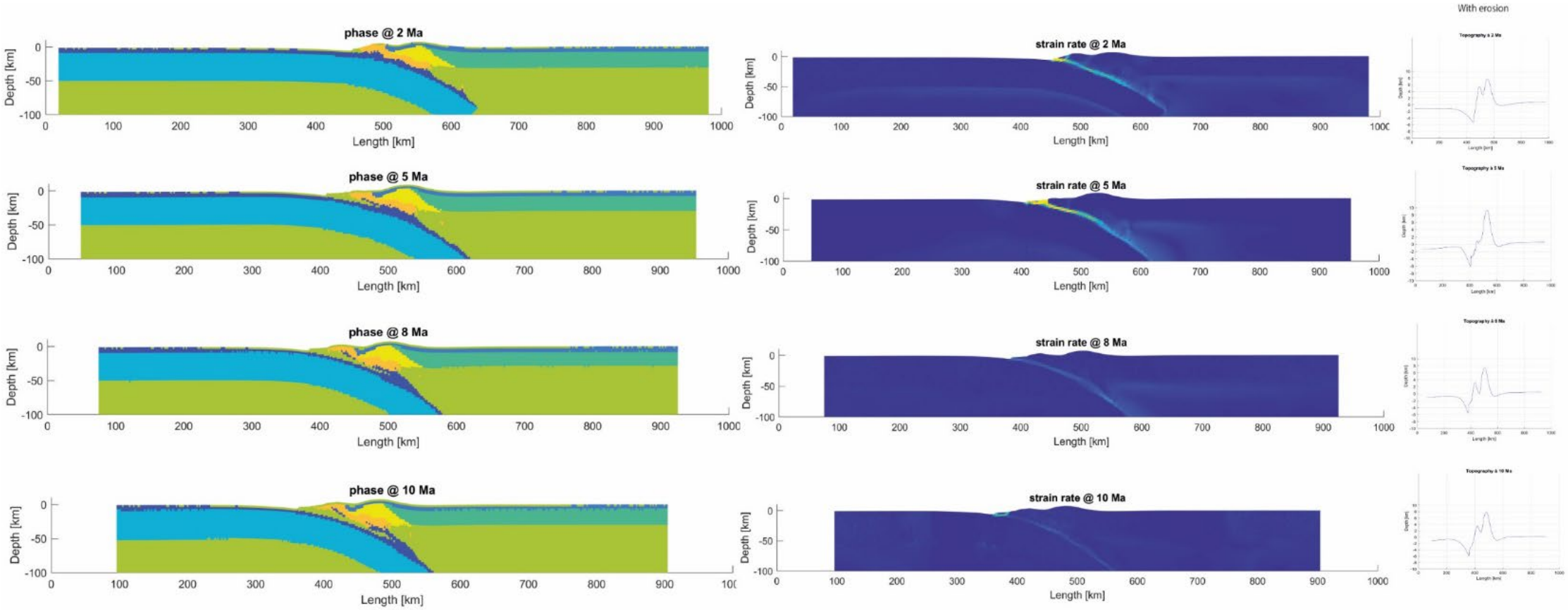

Figure 11 - the diagrams show the typical evolution of a shallow slab model. This model has a thick serpentinite wedge (yellow). The serpentinite wedge shows the shape of a diapir after 2Ma. An accretionary wedge is formed from the sediments on the plate interface. The rest of the sediments ends up underneath the diapir. Erosional products end up in the wedge.

3.3 Description of serpentinite samples

Sample 7.2, 7.5H and 7.5S have a serpentinization degree of over 90% (figure 12). The dominant serpentine mineral is lizardite and minor chrysotile is found. Only minor spinel remains in the three fully serpentinized samples. In sample 7.5S, minor pyroxene can be found as well. Sample 7.3 has a lower serpentinization rate (~70%). Large crystals of diopside, enstatite and forsterite remain (figure 12f). All four samples contain magnetite, but magnetite is considerably less abundant in sample 7.3 compared to the others. Magnetite is found in serpentine veins, as small accumulations and in the mesh texture. Sample 7.2 contains minor Ti-poor titanite.

The samples contain abundant mesh texture. The mesh is sometimes disturbed, or has been replaced by isotropic serpentine. The places where pyroxenes used to be, bastite textures can sometimes be found. In sample 7.3, original grain shapes can still be recognized(figure 12d and f). This is usually not the case in the other three samples.

In the samples with a high serpentinization degree, there are many veins, that cross-cut each other. The larger veins are often crack-seal veins. The small veins are never crack-seal veins. The composition of the veins changes: it can either be serpentine (often chrysotile) and magnetite. Magnetite veins are often cut by smaller serpentine veins. Carbonate veins are only found in sample 7.3 and it has a composition ranging from calcite to dolomite. In sample 7.5H, younger veins are observed to 'meander' through an older, larger vein, instead of forming a crack-seal type vein.

4. Discussion

The results allow me to discuss the uplift of the Troodos Mountains with field data, numerical modelling and serpentinite samples. First, the results of the fieldwork will be interpreted in order to calculate uplift rates and link them to different uplift mechanisms. Then the models will be discussed, first generally, then with respect to the Troodos. After, the serpentinites will be interpreted. Then the three data types will be integrated.

4.1 Identifying and quantifying constraints on phases of uplift

4.1.1 Troodos uplift phases of the past 9-0Ma from field observations

The results of the clast analysis in the fan deposits reveal multiple uplift and erosion phases of the Troodos ophiolite. The first uplift phase (9-6.5Ma) occurred during the Miocene when the Pakhna fans were deposited. The reefal limestones of the Pakhna formation indicate shallow water conditions, which imply a dramatic lowering of the sea level after the deep sea deposition of the Lefkara formation, which likely results from tectonic uplift. The uplift phase is interpreted to have started at 9Ma, because of major changes in plate tectonics and the onset of transpressive strike-slip deformation at that time (Dewey et al., 1989; Harrison et al., 2004).

The Pakhna formation is followed by the Kalavasos Formation (6.5-5.3Ma), which is interpreted as a period of relative tectonic quiescence due to the absence of submarine fans. As the Kalavasos formation consists of evaporite deposits, it could be argued that the relative sea level fall responsible for these deposits is of tectonic origin. The Kalavasos rocks are deposited as a result of the Messinian Salinity Crisis: the temporary closing of the Strait of Gibraltar blocked the influx of water from the Atlantic, and subsequently more water in the Mediterranean evaporated than entered the area, resulting in deposition of evaporites (Krijgsman et al., 1999). Therefore, the absence of fans and mass waste deposits makes it difficult to quantify what amount of relative sea level fall is the result of either uplift or the closing of the Strait of Gibraltar. As no submarine fans are studied, the interval from 6.5-5.3Ma is interpreted as a period of little to no uplift.

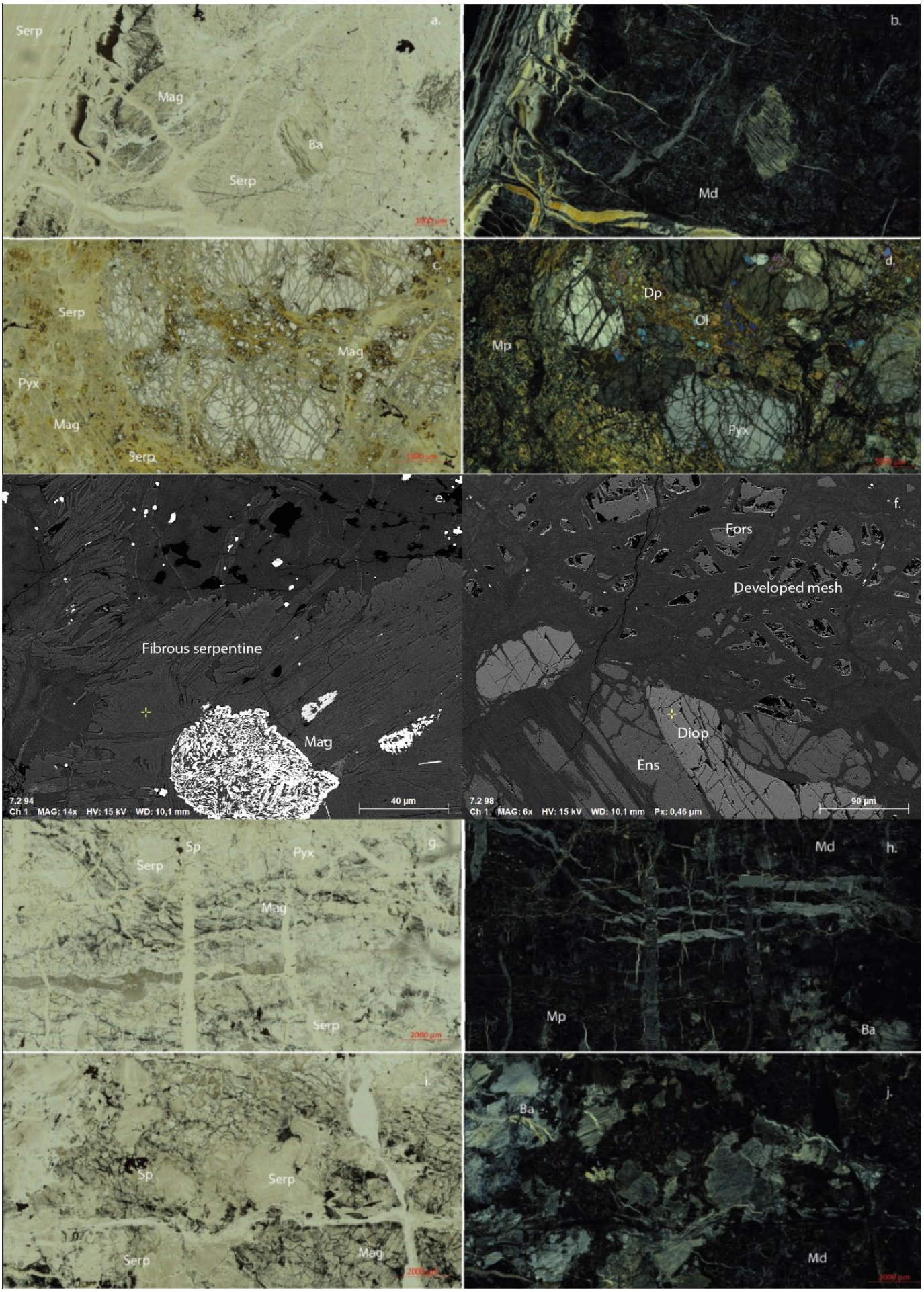
a.
Serp
Mag
Ba
Serp
b.
Md
c.
Serp
Mag
Pyx
Mag
Serp
d.
Dp
Ol
Mp
Pyx
e.
Fibrous serpentine
Mag
40 µm
7.2 94
Ch 1 MAG: 14x HV: 15 kV WD: 10,1 mm
f.
Fors
Developed mesh
Diop
Ens
90 µm
7.2 98
Ch 1 MAG: 6x HV: 15 kV WD: 10,1 mm Px: 0,46 µm
g.
Sp
Serp
Pyx
Mag
Serp
h.
Md
Mp
Ba
i.
Sp
Serp
Serp
Mag
j.
Ba
Md

Figure 12 - a. PPL image of sample 7.2; b. XPL image of sample 7.2 c. PPL image of sample 7.3; d. XPL image of sample 7.3; e. back-scatter image of sample 7.2 (a and b); f. back-scatter image of sample 7.3 (c and d). g. PPL image of sample 7.5H; h. XPL image of sample 7.5H; i. PPL image of sample 7.5S; j. XPL image of sample 7.5S. Serp = serpentinite; mag = magnetite; ba = bastite texture; md = disturbed mesh texture; mp = perfect mesh texture; pyx = pyroxene; dp = diopside, ol = olivine; ens = enstatite; diop = diopside, fors = forsterite, sp = spinel.

The next uplift phase (5.3-2.5Ma) occurred in the Pliocene, leading to the deposition of the Nicosia fans. The variation of clasts is different from the initial Pakhna fans. The increase in the mafic pillow basalts and microgabbros (originating from the intruded dikes that constitute the upper part of the ophiolite), implies that those parts of the Troodos ophiolite were exposed. Only one of the youngest Nicosia fan deposits contained a few gabbro clasts, which indicated that towards the end of the Pliocene, the sheeted dykes were eroded sufficiently to expose the deeper gabbros. Multiple studies (McCallum, 1989; Rouchy et al., 2001; Stow et al., 1995) find that the first emergence above sea level of the pillow lava and microgabbro formations occurs in the late Miocene to early Pliocene. This is in agreement with my findings.

During deposition of the Kakkaristra formation (2.5-2.0Ma), in the late Pliocene to early Pleistocene, the limestone content of the fans decreased, which could be the result of 1) complete erosion of the Pakhna and Lefkara formations; or 2) minor reworking of previously deposited fans, or 3) the close distance of deposition of the Kakkaristra formation to the core of the ophiolite, which potentially overlies the Pakhna and Lefkara limestones. An increase in sheeted dike and gabbro clasts shows that these two formations are prominently exposed and eroded during the deposition of the Kakkaristra fans. McCallum (1989) also finds gabbro in the late Pliocene conglomerates (Kakkaristra Fm).

The youngest alluvial fan deposits, the Fanglomerates, are deposited between 197 ka and 11.7 ka, and are more widespread throughout the region. The highly variable content of mafic and limestone clasts suggests that these rocks are resistant to weathering and thus remain in the fan deposit. The smaller clast size and more rounded clast morphology could be an indication that the clasts originate from reworked older fans or that they have a more distal source compared to the older conglomerate deposits. An increase of the percentage of umber clasts in this fan deposit is probably a result of the high weathering resistance of silicified rocks, meaning that they much longer survive, compared to gabbros and softer ultramafic rocks. Some studies have found that the percentage of gabbro clasts increases in fans deposited during the late Pleistocene compared to those deposited in the Pliocene (McCallum, 1989; Poole & Robertson, 1991, 1998). This is inconsistent with the results of this study, as I find that the amount of gabbro clasts decreases compared to the late Pliocene. This could be the result of the rapidly weathering nature of gabbro or lower uplift and subsequent erosion rates.

No ultramafic material was found in any of the fans surrounding the Troodos ophiolite. Multiple studies did find ultramafic clasts in fans in the lower Pleistocene, albeit very locally: ultramafic clasts have been found in the northwest only in drilled samples taken from the riverbed of the Karyotis river (Poole & Robertson, 1991, 1998; Stow et al., 1995). The conclusion of these studies is that the ultramafic sequence of the Troodos probably was exposed during the early Pleistocene, because ultramafic clasts are found in conglomerates, even though they are not very abundant. The ultramafic clasts are thus found in deeper conglomerates, which are now overlain by younger ones that do not contain ultramafic clasts, hence why they do not outcrop in the field.

4.1.2. Uplift rates of the different uplift phases

To calculate the uplift rates of the above identified uplift phases, I have made two assumptions. The first assumption is that uplift has started near the end of the Miocene, because the first submarine fans I have studied are found in the Pakhna formation. Therefore, I assume that uplift initiated at 9Ma during deposition of the Pakhna when major tectonics in the Mediterranean changed (Dewey et al., 1989; Harrison et al., 2004). The second assumption is the thickness of the layers. In table 5, I have listed the minimum and maximum thickness of the separate stratigraphic and crustal units. Those thicknesses are retrieved from referenced literature.

Table 5 - Ages of deposition and thicknesses used to calculate the uplift rates. Minimum and maximum uplift is cumulative and is inferred from the erosional products. 1: (McCallum, 1989) ; 2: (Zomeni, 1977) ; 3: (Kinnaird & Robertson, 2013); 4: (Harrison et al., 2004); 5: (Calon et al., 2005); 6: (Hernández-Molina et al., 2022); 7: (Chen & Robertson, 2019); 8: Cyprus Geological Survey; 9: (Young, 2014); 10: (Mackenzie et al., 2006).

Formation	Time of deposition	Min. thickness (m)	Max. thickness (m)	Min. uplift (m)	Max. uplift (m)
Fanglomerate	1.8-0.01	12[1]	90[2]	5820	10435
Apolos	2.0-1.8		50[3]		
Kakkaristra	2.5-2.0		100[3]	3320	6435
Nicosia	5.3-2.5	100[4]	350[5]	2820	4435
Kalavasos	6.5-5.3		20[3]		
Pakhna	9-6.5	300[6]	400[6]	700	1500
Lefkara			750[6]		
Kannaviou			750[7]		
Peradephi		20[8]	35[8]		
UP + LP + BG			600[9]		
SDC			800[10]		
Gabbro + Plg		3000[10]	6000[10]		

The first uplift phase at the end of the Miocene required 700-1100m uplift (table 6 and 7, Eaton & Robertson, 1993) in order for the Pakhna formation to become subaerial in 2.5myr. The Pakhna formation itself is between 300-400m thick. This means that during the Pakhna, the largest amount of uplift possible without eroding the Lefkara formation is 400+1100=1500m. The minimum amount of uplift would mean that the Pakhna formation is barely subaerial, which results in a minimum uplift of 700m. The accompanying uplift rate is 0.03-0.05 cm/yr. The first uplift phase is interpreted to be the result of changes in major tectonics in the Mediterranean region (Dewey et al., 1989), which resulted in transpressive strike-slip tectonics in Cyprus (Harrison et al., 2004). Uplift could then be the result of the shortening component of the tectonic regime. Uplift rates for this first phase are relatively low, which could be the result of the simultaneous emplacement of the Kyrenia range (Robertson & Kinnaird, 2016), that caused subsidence in the Mesaoria basin (McCallum & Robertson, 1995; Robertson, 1977). Therefore, it could be that uplift of the north of the Troodos was hindered by emplacement of the Kyrenia range and subsequent subsidence.

The second uplift phase between 5.3-2.5 Ma led to the deposition of the Nicosia formation, which required the exposure of the Pakhna, Lefkara, Kannaviou and Peradephi formations. Depending on if the microgabbro was fully eroded or only partially, the amount of cumulative uplift since deposition of the Pakhna formation would be between 2820-4435m (table 6 and 7). The uplift rate of this phase is therefore between 0.08-0.10 cm/yr. The second uplift phase is interpreted to be the result of modern subduction initiation (Kempler, 1998), as the apatite (U-Th)/He ages of Morag et al. (2016) suggest that modern subduction started approximately at 6 ± 2 Ma, which is coincident with the second uplift phase from this study. Other studies have also shown that at ~5Ma, regional tectonics changed from transpressive to contractional (Harrison et al., 2004), which fits with the interpretation of modern subduction initiation as well. Uplift rates for this phase remain low, which could still be a result from emplacement of the Kyrenia range, as subsidence continued into the Pliocene (McCallum & Robertson, 1995; Robertson, 1977).

Table 6 - Minimum uplift rates calculated for the four uplift phases. dH is the difference between the cumulative uplifts of the current and previously deposited formation.

Formations	Time in myr	Cumulative uplift in m	dH (min)	Uplift rate in m/myr	Uplift rate in cm/yr
Fanglomerate	1.8	5820	2500	1489	0.15
Kakkaristra	0.5	3320	500	1000	0.1
Nicosia	2.8	2820	2120	757	0.08
Pakhna	2.5	700	700	250	0.025

Table 7 - Maximum uplift rates calculated for the four uplift phases. dH is the differencen between the cumulative uplifts of the current and previously deposited formation.

Formations	Time in myr	Cumulative uplift in m	dH (max)	Uplift rate in m/myr	Uplift rate in cm/yr
Fanglomerate	1.8	10435	4000	2222	0.22
Kakkaristra	0.5	6435	2000	4000	0.4
Nicosia	2.8	4435	2935	1048	0.1
Pakhna	2.5	1500	1500	536	0.054

The third uplift phase, which took place between 2.5-2.0Ma, resulted in the deposition of the Kakkaristra formation. Assuming that gabbro was only fully exposed during the Pleistocene the maximum uplift would be 6435m (table 7), if I assume the complete gabbroic sequence is eroded. If only the top is eroded, the minimum uplift would be 3320 m (table 6). The uplift rate of this phase was likely between 0.1-0.4 cm/yr. The third uplift phase is interpreted to be the result of the underthrusting of the Eratosthenes seamount (Robertson, 1998b). Underthrusting of the Eratosthenes could have contributed to uplift either through crustal thickening (Ring & Pantazides, 2019) or through added buoyancy, as the continental seamount is a carbonate platform (Robertson, 1998b), which has a reduced density compared to the oceanic crust of the overriding plate. The third uplift phase has also seen the most rapid uplift rate, compared to the first two. This could be the result of the Kakkaristra formation being deposited after emplacement of the Kyrenia range has ceased (McCallum & Robertson, 1995), so that uplift is not minimized by simultaneous subsidence in the Mesaoria basin. Another possibility for an increased uplift rate is that there is a larger component of horizontal compression when continental crust underthrusts,

compared to when denser oceanic crust subducts, resulting in more crustal stacking and thus vertical uplift (Jarrard, 1986).

The fourth uplift phase took place between 1.8-0.01Ma. Minimum amount of cumulative uplift would be 5820 m and maximum amount of cumulative uplift 10435 m. The uplift phase resulted in uplift rates of 0.14-0.22cm/yr. Uplift rates for the fourth uplift phase are smaller than those calculated for the third uplift phase, but are still an order of magnitude larger than those of the Miocene and Pliocene. This implies that underthrusting of the Eratosthenes seamount is ongoing during this phase.

Morag et al. (2016) have calculated a post-Pliocene average uplift rate of 0.86 cm/yr using thermal modelling of a pegmatitic gabbro sample. This is significantly higher than the average uplift rate of the third and fourth uplift phase of 0.13cm/yr (for minimum rates) and 0.3cm/yr (for maximum rates) that results from this study. One reason for this difference could be that the uplift rate from Morag et al. (2016) is calculated for the ultramafic core of the Troodos, whereas ours is calculated based on the circum-Troodos sediments, specifically in the Mesaoria basin. It is possible that the ultramafic core of the Troodos has seen an additional, buoyancy-induced uplift. This would fit with the interpretation of previous studies that solely the buoyancy force of the Troodos serpentinite would not be enough to uplift the entire Troodos, but that it might be enough to uplift Mount Olympus slightly more compared to its surroundings (Ring & Pantazides, 2019; Shelton, 1993). It could also be that isostatic adjustment played a larger part in the area of Mount Olympus (Evans et al., 2021), also contributing to more rapid uplift rates. Another possible contribution to the higher uplift rates at the core is the volumetric expansion of serpentinite, which probably did not taken place in the circum-Troodos area, because meteoric water was not as able to reach the peridotite here.

Generally the uplift rates show that, although uplift has started in the Miocene, its rate increased after the Pliocene: uplift rates of the late Pliocene and Pleistocene are an order of magnitude higher than Miocene values. These increased uplift rates therefore show that subduction, including initiation and collision with the seamount in the trench, is the most dominant uplift mechanism for recent (>9Ma) uplift of the Troodos ophiolite.

4.2 Numerical models

The amount of uplift interpreted from the fieldwork shows that Cyprus has experienced 5.8-10.4km of uplift in the past 9Ma. When comparing the calculated amount of uplift from section …. with the estimate of 17.5km of uplift done by Evans et al. (2021), I find that 7.1-11.7 km of uplift cannot be explained in the past 9Ma. For this reason, earlier processes are needed, perhaps related to the obduction, to explain this uplift. Therefore, the models are discussed to see which mechanisms could have played a role during the process of obduction.

4.2.1 Output

Mechanisms contributing to uplift

Depending on which rheological classification of serpentinite used, the serpentinite can lead to 5-14km of topography within 5myr. The uplift created in 5myr is accommodated by the formation of an accretionary wedge, in which the sediments of the subducting plate undergo frontal off-scraping. These sediments then accrete to the overriding plate, creating back thrusts in the overriding plate's lithosphere itself. When serpentinite is present, the back thrusts form on either side of the serpentinite wedge. An explanation for this quick formation of an accretionary wedge is the difference in cohesion of the sediments, which is $1/8^{th}$ of the cohesion of the other materials used, making it relatively easy for the material to be pushed up. In addition to that, the weak

sediments have low coupling with the stronger oceanic crust of the slab and weak coupling creates accretionary margins instead of erosive ones (Pusok et al., 2021). Other explanations for the margin being accretionary and not erosive, are that it is possibly the result of the convergence rate and sediment thickness. The convergence rate is smaller than 6cm/yr, and the sediment thickness is larger than 1km, which results in an accretionary margin (Clift & Vannucchi, 2004). In the models, the sediment in front of the overriding plate gets scraped off, the material that is underneath underplates. Sometimes, the underplating material's buoyancy causes the serpentinite above to form a domal structure. In this way, the underplating material also contributes to uplift.

As maximum elevation is reached within 2-3myr, after which the peak subsides and thus the elevation after 10myr is lower than the maximum elevation. This implies that actual uplift is a short-lived, quick process. This could be the result of very localized deformation, shown in the localized strain rates of the models (figure 10 and 11). Localized strain allows quick uplift in a short period of time because deformation is focused in a small area. Previous research has shown that localized uplift happens when a weak interface layer is present (Koptev et al., 2022), which is the case in this study's models. Both plates have a weak layer: the sediments on the downgoing plate and the serpentinite (present in most models) in the overriding plate, enabling decoupling between the two plates. Decoupling between the two plates causes localized strain and thus rapid uplift.

After formation of the accretionary wedge, the models start to subside. The subsidence phase is faster in models without serpentinite. In those models, less than 50% of maximum elevation remains after 10 myr, compared to 60-80% of the elevation being retained for the models with serpentinite after 10 myr. The subsidence could be due to gravitational collapse of the recently formed topography, as the newly formed peaks have high gravitational potential energy. However, this would not explain why the serpentinite models experience slower subsidence, as in all situations, high topography is formed. The subsidence could therefore also be the result of buoyancy differences, as the lighter density of serpentinite makes the material more buoyant than unserpentinized peridotite. The buoyancy of serpentinite creates an upward force, which results in slower subsidence of the created elevation. Another possible reason for slower subsidence when serpentinite is present is isostatic adjustment: as the serpentinite has a smaller density than the unserpentinized peridotite, the gravitational equilibrium is different for the models with and the models without serpentinite. For a model with serpentinite, the point of gravitational equilibrium is possibly higher than for a model without serpentinite, which thus reduces the amount of subsidence necessary to achieve equilibrium.

Uplift rates of the models range between 0.09-0.9cm/yr, which all fall within the range for uplift rates in the natural realm. Uplift rates are more controlled by subduction angle than by serpentinite density and thickness. The models show that shallow slabs create low uplift rates but high elevation, whereas steep slabs create high uplift rates but low elevation. This could be due to the difference in coupling between the subducting and overriding plate. A low subduction angle creates a larger contact area compared to a steep slab. The larger contact area creates a higher degree of coupling between the two plates, which in turn can create more uplift by creating a larger stress field and stronger upper plate deformation (Huangfu et al., 2016). Another way is that a larger contact area promotes the transferral of stress to the upper plate (Jordán et al., 1983), again creating more deformation in the form of uplift in the upper plate. A shallower dip can thus reduce the effect that buoyancy has on the topography (Hu & Gurnis, 2020), as the models with the lowest uplift rates all contain serpentinite and most of them have low density serpentinite too.

Models without serpentinite have the lowest elevation after 10myr. An explanation for the link between greater elevation and the presence of serpentinite could be that serpentinite is more buoyant than regular mantle peridotite and therefore, the serpentinite enables decoupling between the plate interface and the mantle wedge. In the models of Porkoláb et al. (2021) the greater buoyancy of the continental crust enables it to decouple from the rest of the subducting lithosphere. Another reason for the increased elevation by the serpentinite models could be that the rheology of the mantle wedge changes when it is serpentinized: its frictional strength is reduced then because of elevated pore fluid pressure (Wada et al., 2008). Less friction in the mantle wedge means that there are less forces counteracting the forces of the subducting slab, which could result in higher topography (Conrad & Hager, 1999). In addition to that, the frictional strength of the plate interface determines the behaviour of the accretionary wedge: low friction has a high accretionary wedge, whereas high friction means the wedge becomes non-existent (Tan et al., 2012). In general, overriding plate topography is controlled mostly by rheology, followed by slab dip and only then buoyancy (Crameri et al., 2017).

Ophiolite emplacement

There are ten models in which a thick serpentinite diapir can be seen to cut off a part of the overriding plate's crust after 8-10 myr. This piece of oceanic crust then remains on top of the accretionary wedge. The process of necking and breaking in these models that create an ophiolite is very similar to the process observed by Porkoláb et al. (2021) in their models. In these models, the process of necking and breaking is observed after over 20 million years as a consequence of buoyancy-induced decoupling of the subducting continental crust (Porkoláb et al., 2021). The difference in time that it takes to create an ophiolite sheet between my models and theirs is at least 10myr. This difference could be due to two things: 1) in my models, the serpentinized mantle wedge is already present at the start of the model and in theirs, the continental crust has not yet subducted at the start, which thus takes time to take place; 2) the three types of serpentinites that I have used in my models all have lower densities than the continental crust used by Porkoláb et al. (2021). Therefore, the material that subducts in my models is more buoyant compared to the oceanic lithosphere used than the material used by Porkoláb et al. (2021), which could result in faster decoupling and thus faster necking and breaking of the overriding oceanic lithosphere.

In the models of this study, the accretionary wedge helps in transporting the ophiolite across the subduction zone: the little basin between the accretionary wedge and the serpentinite diapir aids in providing a shelter for the oceanic crust during transport. Previous study has stated that three things are necessary for ophiolite emplacement: 1) 350-400km of shortening; 2) the presence of strong felsic crust; 3) the presence of a thermal anomaly (Duretz et al., 2016). The findings of this study do not agree with those points: the models have undergone less than 300km of shortening, no felsic crust is present, as well as no thermal anomaly. Instead, the two buoyant structures formed by the accretionary wedge and the serpentinite diapir create a protective basin for the oceanic crust to safely get transported before emplacement on the subducting plate. This shows that continental crust is not necessary for ophiolite emplacement. Of greater importance is the buoyancy and age of the crust, as young and buoyant crust is receptive for ophiolite emplacement and preservation (Woelki et al., 2019). The young crust in this study's models is therefore easily lifted across the trench by the buoyancy of the serpentinite diapir and accretionary wedge.

Ophiolite emplacement is mainly observed in models with thick serpentinite wedges (15km). In models with dense or thin serpentinite, necking and breaking of the crust sometimes occurs, but transport is difficult without the presence of a serpentinite diapir. As none of the processes involved in ophiolite emplacement are observed in models without serpentinite, it shows that serpentinite diapirism is crucial in ophiolite emplacement in these models. In all models, an

accretionary wedge forms, but in models with thin, dense or no serpentinite, the accretionary wedge is unable to transport and emplace the ophiolitic crust itself.

4.3 An integrated model for uplift of the Troodos ophiolite

As 17.5km has been estimated as a number for total uplift in the Troodos (Evans et al., 2021), and the fan deposits have documented 5.8-10.4km of uplift, 7.1-11.7km of uplift is not accounted for by the Neogene and Quaternary uplift mechanisms. Therefore, the models and the mechanisms through which they enable uplift are applied to the case of the Troodos ophiolite, in order to improve understanding of early processes in the uplift history.

Six models have generated 7-11km of uplift after ten Ma. Five of these models have shallow slabs, medium to thick serpentinite with a low to medium density. Uplift rates of these models are within 0.1-0.3 cm/yr. The sixth model, model 25, has a steep angle, light density serpentinite in a thick serpentinite wedge and an uplift rate of 0.9cm/yr, which is the highest uplift rate of all models. Of all six models, model 25 is most applicable to the situation of Cyprus, following this reasoning: the Troodos crust was very young when it got obducted (Blome & Irwin, 1985); and younger slabs have steeper subduction angles (Hu & Gurnis, 2020).

Model 25 is a model with a steep slab that shows very fast uplift of 9km in the first million year. After this, the model experiences little subsidence and after ten Ma, 7km of the topography remains. The fast initial uplift is due to the serpentinite forming a diapir and then rising quickly. Due to its buoyancy, the serpentinite does not subside as quickly as it rises. The serpentinite's diapirism starts the process of necking and breaking, similar to that observed in Porkoláb et al. (2021): after 10 Ma, a sliver of oceanic crust has partially broken off from the overriding plate. The strain is localised on the plate interface. Minor strain is focused on the two borders of the serpentinite diapir. The serpentinite inside the diapir is undeformed. Model 25 shows that the modelled young subduction system was able to create an ophiolite, through formation of an accretionary wedge and a serpentinite diapir. These buoyant structures both aided in transporting the overriding oceanic crust over the trench.

The models, including model 25, show that thick serpentinite wedges are necessary for ophiolite emplacement through serpentinite diapirsm. The Troodos serpentinites are ~10-15km thick in diameter (figure 6). Therefore, the diameter of the serpentinite diapir in the Troodos is sufficient to have aided in ophiolite emplacement. The second element needed in the models for ophiolite emplacement, is an accretionary wedge. In the case of Cyprus, the Mamonia Complex has been interpreted as an accretionary wedge (Chan et al., 2007). The two faults bordering the serpentinite diapir in the model have been observed to border the Troodos serpentinite as well (Evans et al., 2021). Therefore, model 25 shows that emplacement of the Troodos ophiolite could have been made possible through the combined efforts of the serpentinite and the Mamonia complex, in which the buoyancy of the Troodos serpentinite aided in initial uplift and breaking of the crust, and the Mamonia complex aided in transporting the crust across the subducting zone. After emplacement, the serpentinite could have aided in maintaining uplift through isostatic adjustment.

4.4 Identifying thermal and tectonic conditions from the serpentinite samples

The field data and numerical modelling allow the identification of the different uplift phases and the quantification of the uplift rates. The serpentinite samples can provide thermal constraints and physical conditions by looking at the mineral assemblages and microtextures of the samples, that accompany the tectonic evolution of the ophiolite. Since only four serpentinite samples of the Troodos and Limassol forest were studied, it remains difficult to find depth indicators. However,

temperature constraints could be extracted, which allow me to place the serpentinization within the tectonic history of the ophiolite.

Thermal conditions

There are multiple indications that the majority of the serpentinization reactions in the serpentinised samples took place in low temperatures conditions (200-400^0 C), with the possibility to be overprinted by later serpentinization of different temperatures.

Olivine disintegrates preferentially at temperatures of 250-300^0 C, whereas orthopyroxene disintegrates preferentially at temperatures larger than 400^0 C (Martin & Fyfe, 1970). Since all of the samples have a high grade of serpentinization, only a few samples contain pyroxenes, and as even less forsterite is found, it shows that olivine has been altered more than the pyroxenes, suggesting lower (250-300^{0}C) temperatures for the serpentinization process. In addition, all samples contain mostly lizardite and chrysotile which also implies lower temperatures because lizardite and chrysotile are stable at relatively shallow depths and low temperature (<400^0 C) (Mével, 2003). Lastly, the absence of antigorite in the samples implies that the upper limit of the temperature is 400^{0}C during fluid infiltration (Skelton & Valley, 2000), because antigorite is the high-pressure/high-temperature polymorph of the serpentinite minerals. Therefore, an absence of antigorite shows that the temperature has not exceeded 400^{0}C during serpentinization of these samples.

Another mineral that can provide information on the temperature condition is brucite, which was not found in any of the samples. The lack of brucite in the samples can be due to 1) the serpentinite having formed in a chemically open system; 2) the brucite having already dissolved and weathered due to the high degree of serpentinization (Bach et al., 2006; Schwarzenbach et al., 2016). If the serpentinization rate is higher than 60%, the weathering of the Fe^{2+} in brucite can result in a fast increase in magnetite (Bach et al., 2006). This is likely to be the case in the samples, as serpentinization exceeds 60% in three out of four samples, and abundant magnetite is found.

Magnetite is the third most prevalent mineral, after lizardite and chrysotile, that can provide information on the thermal conditions. In all samples, magnetite is found both in veins and in the mesh making all samples very rich in magnetite. Therefore, the lower limit of the formation of the serpentinites has to be 200^{0}C, as magnetite does not form in such large quantities if the temperature is lower than 200^{0}C (Bonnemains et al., 2016; Cox et al., 2021; Klein et al., 2014).
Magnetite increases with increasing degree of serpentinization (Oufi et al., 2002). Thus, the difference in magnetite content between sample 7.3 and the other three samples could be the result of the lower serpentinization degree in sample 7.3.

The microstructure of the serpentine samples also informs us about the thermal conditions. The most prevalent microstructure in the samples is the mesh texture, which implies that the samples are mostly undeformed and lizardite is the most prevalent mineral. In addition to that, the sample from the Limassol Forest Complex contains bastite textures, which suggests temperatures of 300-400^{0}C (Agrinier & Cannat, 1997) and potentially a slightly deeper origin of the serpentinised material.

Water-rock ratio

The presence of chrysotile, magnetite or calcite in the veins shows that water-rock ratio was high during formation of those veins (Prichard, 1979). Generally, the cross-cutting relationships between multiple generations of veins, as well as the bandedness within veins, and the recrystallization of different minerals within the veins show that the veins document a complex

history of continuing and increasing serpentinization within the rock and hereby overprint previously formed microtextures such as the mesh.

Tectonic conditions

Since my samples consist predominantly of lizardite and minor chrysotile, which are common minerals during peak serpentinization processes in ocean floor formation and detachment fault activity (Mével, 2003), it is a first indication that the highest degree of serpentinization occurred in an extensional or oceanic spreading tectonic setting. In a fore arc wedge and in a subduction zone setting, the dominant serpentine mineral is antigorite (Guillot et al., 2015) and so the lack of antigorite in the samples implies that bulk serpentinization did not take place during subduction. In addition to that, serpentinites that form in a fore arc mantle wedge contain chlorite-bearing harzburgites and are associated with eclogites (Guillot et al., 2015). These types of mineral assemblages are both not found in our samples or in close proximity in the rest of the Troodos, which is another indication that the tectonic conditions were different from the fore arc domain.

As described in section 3.2.1, minor antigorite is found in the Troodos ophiolite, but it was not found in the samples discussed here. A minor amount of antigorite is also found in other Limassol Forest serpentinite samples (Cox et al., 2021). Cox et al. (2021) concluded that these serpentinites must have formed at conditions where all of serpentine polymorphs are stable, which is in the range of 300-400^{0}C, i.e. the lower greenschist facies conditions (Cox et al., 2021). As antigorite is not the dominant serpentine mineral but is found in minor quantities in the Troodos and the Arakapas fault zone, it could be that there was a second, higher pressure/higher temperature serpentinization phase. It is possibly that some of the serpentinite minerals in this region were recrystallised into antigorite. Still, the bulk of the serpentine minerals found in the Troodos ophiolite formed in low-pressure, low-temperature conditions, which are more likely to happen in a mid-ocean ridge, than in a subduction zone setting.

A possible explanation for the large amount of serpentinite found on Cyprus is that the first phase of serpentinization started after formation of oceanic crust in an extensional supra-subduction setting. The slow spreading ridge in which the crust formed (Morris & Maffione, 2016) provided enough fluids, but also enough faults (e.g. the Amiandos fault (Nuriel et al., 2009) and the fossil Arakapas transform fault) to accommodate fluid penetration into the rock. Due to the very slow spreading rate, the conditions could have remained stable over a longer period of time throughout the region, which resulted in a large area experiencing a high degree of serpentinization. The minor antigorite then shows a next phase of serpentinization, under higher pressure and temperature conditions compared to the first phase.

Then there are also the strong indicators (e.g. Evans et al., 2021; Magaritz & Taylor, 1974; Nuriel et al., 2009) that the serpentinites are at least partly formed by meteoric waters. Other studies have interpreted this indicator as an evaporitic signature and associated it with underthrusting of the seamount (Robertson, 1990). Both interpretations indicate that a third serpentinization phase is plausible, which is likely still ongoing. Therefore, serpentinization through meteoric waters is interpreted to be a recent phase in the serpentinization process. It is, however, difficult to attribute to which phase meteoric serpentinization belongs. Recent erosion of the overlying rocks of the oceanic crust, may have created a pathway for fluids into the ultramafic core of the ophiolite, leading to more serpentinization and a more rapid increase of the uplift rate. It may also be that the underthrusting of the Eratosthenes seamount has contributed to fluid influx in the system. In both cases, serpentinization through meteoric fluids could have taken place in both the third and fourth uplift phase. The serpentinization could have aided uplift through volumetric expansion of the rocks and isostatic readjustment.

4.5 The tectonic evolution of the Troodos ophiolite

The serpentinite samples show a very high percentage of low pressure/low temperature serpentinization, meaning that the majority of serpentinization most likely took place near the spreading centre, prior to the obduction and uplift of the Troodos mountains. The abundance of magnetite also implies that bulk serpentinization has happened in close proximity to the ridge. This implies that the majority of serpentinization happened soon after formation of the crust. The Troodos crust has a supra-subduction zone geochemical signature, resulting from the crust initially forming above a subduction zone (Osozawa et al., 2012). Soon after formation, water entered this newly formed crust and serpentinization reactions began. After this, the serpentinite decoupled from the lithosphere and ascended as a diapir in the slow-spreading ridge (Evans et al., 2021). During ascension of the diapir, the overlying oceanic crust started breaking. The uplifted oceanic crust was later emplaced onto the subducting plate, possibly through the aid of the Mamonia complex sediments in the accretionary wedge. The initial uplift phase resulted in 7-11km of uplift.

As the serpentinites indicate that the majority of serpentinization reactions has occurred in close proximity to the spreading ridge, it does not seem likely that serpentinization is a major contributor to Neogene and Quaternary uplift, as proposed by Morag et al. (2016) and Evans et al. (2021). The uplift rates have shown that recent uplift can be explained using regional tectonics. Serpentinite diapirism on its own is also not sufficient to fully account for the proposed 17.5km uplift the Troodos has seen (Evans et al., 2021), as the maximum uplift in the serpentinite models from this study is 12.5km. Therefore, tectonic processes are needed to fully complete the timeline of uplift.

The field results have shown that Cyprus has been uplifted 5-10 km over the last ten Ma. The Troodos ophiolite underwent four pulses of uplift in the Neogene and Quaternary. The first phase in the Late Miocene resulted in uplift rates of 0.025-0.054 cm/yr and was probably due to changes in the tectonic regime throughout the Mediterranean (Dewey et al., 1989; Harrison et al., 2004). The second uplift phase with intermediate uplift rates of the Troodos occurred in the Pliocene, during deposition of the Nicosia formation, as a result of compressive tectonics (Harrison et al., 2004) and the onset of modern subduction (Morag et al., 2016). The third and fastest uplift phase took place in the late Pliocene, early Pleistocene and was a result of the incipient collision with the Eratosthenes seamount (Robertson, 1998b). The last uplift phase took place in the Pleistocene and resulted in the deposition of the Fanglomerate formation, when underthrusting of the seamount continued.

What remains unclear, is the age of the antigorite and meteoric serpentinization. The antigorite could have formed in either the Cretaceous or the modern subduction zone. It is therefore unclear whether and how much this serpentinization phase has contributed to uplift. The same reasoning can be applied to the meteoric serpentinization, as it could have contributed to the last two uplift phases.

5. Perspectives

5.1 Limitations of the fieldwork

To study clast content, I have made estimations of the proportions of a certain clast type relative to the total clast content. These estimations were based on how much of this clast type I had found when studying the outcrop. I focused on clasts that were larger than 2cm. This leaves some room for sampling bias, as quickly-weathering clasts might have been underrepresented, whereas very weathering-resistant rocks could be overrepresented in the large clasts. What could have been done, is take a 1x1m square in each outcrop, and then study the composition of all the clasts in the square. The benefit of this is that it is done very precisely, but it takes a lot of time and would have

resulted in being able to study less fans, and thus having a less comprehensive data set to infer the uplift phases from.

Secondly, the calculation of Neogene and Quaternary uplift rates is based on thicknesses of the different formations. Some estimations of thicknesses of certain formations varied a lot in estimation, such as the gabbro, which has been estimated to be between 3-6km thick (Mackenzie et al., 2006). This leaves a lot of room for uncertainty, which could have influenced the cumulative uplift calculations.

One assumption that has been made while integrating the field and model data, is the depth form which the Troodos serpentinites have come and how much uplift the Troodos in total has seen. It is more or less possible to calculate the minimum and maximum uplift of the Troodos up to the gabbros, as estimations of the formation's thicknesses are available. There are, however, no depth markers of the Troodos serpentinites, nor is it known how much uplift the Troodos exactly has seen. Therefore, in this study, I used the estimation done by Evans et al. (2021) of 17.5km to calculate the amount of uplift in the Troodos, on which I based which model fits best for the case of Cyprus. This would have improved if precise depth markers are available. However, the complex history of multiple serpentinization phases prohibits easy inferral of serpentinization depth. It would be interesting to see if future research could find more constrained depth markers of the serpentinite, so that the calculation of how much uplift the Troodos has seen could be more accurate.

5.2 Limitations of the model and future work

In the models, sediments were used as a plate interface material, even though serpentinite could be more realistic. A soft, low density material is needed in between the plates to make sure that movement is possible and the models run stable. If the plate interface material would consist of serpentinite and there is a serpentinite wedge in the overriding plate, there would be two bodies of serpentinite in the model. This would make it harder to see what the influence of the serpentinite wedge is on the topography. Therefore, I think it is not feasible to have used serpentinite as the plate interface material.

In the models, there are no phase changes: the peridotite in the lithospheric mantle does not change to serpentinite during model time. Instead, the serpentinization has already occurred. This is justifiable, as Rouméjon and Cannat (2014) calculate that bodies of peridotite can be serpentinized over a period of 500-1100 days, if there is enough water available. 500-1100 days is near-instantaneous on geological timescales, and especially on the time scale used in these models. For future work, it would be interesting to test models in which a phase transition of peridotite to serpentinite happens during run time of the model, to see how serpentinization influences uplift, when a fully serpentinized mantle wedge is not present yet. This would further improve understanding of the extent and through which mechanisms serpentinization can contribute to uplift and obduction.

Another limitation of the model is that the convergence rates are not true to nature. GPS data has shown that the current velocity with which Africa moves to Eurasia is 2cm/yr (Fernandes et al., 2003). However, when implementing this in the models, the downgoing plate would buckle and strain would be located close the left boundary of the model, instead of in the slab itself. Therefore, the convergence rate is not completely true to the convergence rate between Africa and Eurasia, but was chosen so that the total amount of shortening would remain the same. The models would have been more accurate for the Troodos case if the actual velocity could have been implemented. To do so, different rheological parameters for the subducting plate should have been used, which

now was not possible due to time management, but it would be good to resolve this problem in future models.

Other limitations of the method are that 2D models assume an infinitely long plate, which for Cyprus is not the case. A 3D model setup, might simulate the uplift better. The viscosity in the plate is the same throughout the entire plate, which is not the case in nature. This, again, has to do with the rheological parameters used.

Last, another aspect for future work would be to conduct a parameter test to see in which conditions an accretionary wedge contributes to obduction, and in which conditions it does not. Multiple studies ((Clift & Vannucchi, 2004; Pusok et al., 2021) have been done on when a margin becomes accretionary or erosive, but not many studies have researched those implications in the context of obduction.

6. Conclusion

The aim of this is study is to provide a more comprehensive timeline of the complex uplift of the Troodos ophiolite and its corresponding mechanisms through quantifying the amount of uplift and uplift rates in the multiple phases.

- The serpentinite could have aided the Cretaceous emplacement of the ophiolitic crust through its buoyancy, enabling necking and breaking through decoupling and subsequently lifting the Troodos ophiolite and emplacing it on the accretionary wedge. Then, the buoyancy of the serpentinite and the accretionary wedge ensure emplacement of the ophiolite on the subducting plate. The process of obduction is interpreted as the first phase of uplift, likely resulting in 7-11km of uplift. After a period of relative quiescence, uplift resumed in the Miocene based on the four uplift phases studied in the submarine and deltaic fans. Total uplift from the Miocene to the present-day is 5.8-10.4km. At 9 Ma with uplift rates of 0.025-0.054cm/yr, the Mediterranean region experienced major changes in tectonic regime, resulting in the second uplift phase in Troodos history. At ~5 Ma (0.08-0.10 cm/yr), modern subduction was initiated which resulted in the third uplift phase. The fourth (2.5-2.0 Ma, 0.1-0.4 cm/yr) and fifth (1.8-0.01Ma 0.15-0.22 cm/yr) uplift phases are caused by underthrusting of the Eratosthenes seamount, through understacking and/or influx of meteoric water and subsequent serpentinization.

- The models show the following trends: 1) thick serpentinite creates more topography than thin serpentinite; 2) light serpentinite creates more topography than dense serpentinite; 3) erosion in models with a shallow slab creates lower topography than in models without erosion, whereas in models with a steep slab, erosion creates higher topography than in models without; 4) uplift usually occurs for 2-5 million years, after which subsidence start; 5) steep slab models experience less subsidence when erosion or serpentinite is applied.

- The models show that uplift rates are mostly controlled by subduction angle, and not by serpentinite density and thickness. Uplift is mostly controlled by rheology, followed by slab angle and buoyancy.

- The models show that the serpentinite can contribute to uplift in multiple ways. The first is that the serpentinite enables decoupling, so that strain localizes, causing localized deformation and thus very local uplift. Secondly, serpentinite reduces the frictional strength of a rock through elevated fluid pore pressure, resulting in higher topography.

Thirdly, when topography has been formed, serpentinite can help preserve this, by enabling slower subsidence due to its buoyancy.

- The samples all have a high degree (~70-100%) of serpentinization. All samples contain lizardite, chrysotile and magnetite. Some contain titanite and spinel. One sample contains diopside, enstatite and forsterite. The observed microstructures, relict original minerals and accessory minerals all fit within this temperature range of 200-400^{0}C for the first, bulk serpentinization phase, implying shallow, spreading-ridge related setting. Previous studies have found antigorite in the Troodos serpentinites, and others found a strong meteoric signal in the serpentinite, implying two more serpentinization phases: one in close proximity to the subduction zone and one recent phase where meteoric water could access the ultramafic rock. It remains difficult to identify to which uplift phase the second and third serpentinization phases belong.

7. Bibliography

Agrinier, P., & Cannat, M. (1997). Oxygen-isotope constraints on serpentinization processes in ultramafic rocks from the Mid-Atlantic Ridge (23 N). *Proceeds of the Ocean Drilling Program, Scientific Results*, *153*, 381–388.

Andreani, M., Mével, C., Boullier, A. M., & Escartín, J. (2007). Dynamic control on serpentine crystallization in veins: Constraints on hydration processes in oceanic peridotites. *Geochemistry, Geophysics, Geosystems*, *8*(2). https://doi.org/10.1029/2006GC001373

Bach, W., Paulick, H., Garrido, C. J., Ildefonse, B., Meurer, W. P., & Humphris, S. E. (2006). Unraveling the sequence of serpentinization reactions: petrography, mineral chemistry, and petrophysics of serpentinites from MAR 15°N (ODP Leg 209, Site 1274). *Geophysical Research Letters*, *33*(13), 13306. https://doi.org/10.1029/2006GL025681

Bailey, W. R., Holdsworth, R. E., & Swarbrick, R. E. (2000). Kinematic history of a reactivated oceanic suture: the Mamonia Complex Suture Zone, SW Cyprus. In *Journal of the Geological Society* (Vol. 157). https://www.lyellcollection.org

Batanova, V., & Sobolev, A. V. (2000). Compositional heterogeneity in subduction-related mantle peridotites, Troodos massif, Cyprus. *Geology*, *28*(1), 55–58.

Ben-Avraham, Z., Kempler, D., & Ginzburg, A. (1988). Plate convergence in the Cyprean Arc. *Tectonophysics*, *146*(1–4), 231–240. https://doi.org/10.1016/0040-1951(88)90093-5

Berk Biryol, C., Beck, S. L., Zandt, G., & Özacar, A. A. (2011). Segmented African lithosphere beneath the Anatolian region inferred from teleseismic P-wave tomography. *Geophysical Journal International*, *184*(3), 1037–1057.

Blome, C. D., & Irwin, W. P. (1985). Equivalent radiolarian ages from ophiolitic terranes of Cyprus and Oman. *Geology*, *13*(6), 401–404.

Bonnemains, D., Carlut, J., Escartín, J., Mével, C., Andreani, M., & Debret, B. (2016). Magnetic signatures of serpentinization at ophiolite complexes. *Geochemistry, Geophysics, Geosystems*, *17*(8), 2969–2986. https://doi.org/10.1002/2016GC006321

Brongniart, A. (1813). Essai d'une classification mineralogique des roches mèlangèes. *Journal Des Mines, Paris*, *199*, 5–48.

Burov, E. B. (2011). Rheology and strength of the lithosphere. In *Marine and Petroleum Geology* (Vol. 28, Issue 8, pp. 1402–1443). https://doi.org/10.1016/j.marpetgeo.2011.05.008

Calon, T. J., Aksu, A. E., & Hall, J. (2005). The Oligocene-Recent evolution of the Mesaoria Basin (Cyprus) and its western marine extension, Eastern Mediterranean. *Marine Geology*, *221*(1–4), 95–120. https://doi.org/10.1016/j.margeo.2005.03.012

Cann, J. R. (2003). The Troodos ophiolite and the upper ocean crust; A reciprocal traffic in scientific concepts. *Special Paper of the Geological Society of America*, *373*, 309–321. https://doi.org/10.1130/0-8137-2373-6.309

Caristan, Y. D. (1980). *High temperature mechanical behavior of Maryland diabase.* Massachusetts Institute of Technology.

Chan, G. H. N., Malpas, J., Xenophontos, C., & Lo, C. H. (2007). Timing of subduction zone metamorphism during the formation and emplacement of Troodos and Baer-Bassit ophiolites: Insights from 40Ar-39Ar geochronology. *Geological Magazine*, *144*(5), 797–810. https://doi.org/10.1017/S0016756807003792

Chen, G., & Robertson, A. H. F. (2019). Provenance and magmatic-tectonic setting of Campanian-aged volcaniclastic sandstones of the Kannaviou Formation in western Cyprus: Evidence for a South-Neotethyan continental margin volcanic arc. *Sedimentary Geology*, *388*, 114–138. https://doi.org/10.1016/j.sedgeo.2019.05.002

Clift, P., & Vannucchi, P. (2004). Controls on tectonic accretion versus erosion in subduction zones: Implications for the origin and recycling of the continental crust. *Reviews of Geophysics*, *42*(2). https://doi.org/10.1029/2003RG000127

Clube, T. M. M., & Robertson, A. H. F. (1986). The palaeorotation of the Troodos microplate, Cyprus, in the Late Mesozoic-Early Cenozoic plate tectonic framework of the Eastern Mediterranean. *Surveys in Geophysics*, *8*(4), 375–437.

Coleman, R. G. (1971). Plate tectonic emplacement of upper mantle peridotites along continental edges. *Journal of Geophysical Research*, *76*(5), 1212–1222. https://doi.org/10.1029/JB076I005P01212

Conrad, C. P., & Hager, B. H. (1999). Effects of plate bending and fault strength at subduction zones on plate dynamics. *Journal of Geophysical Research: Solid Earth*, *104*(B8), 17551–17571. https://doi.org/10.1029/1999JB900149

Cox, S., Fagereng, Å., & MacLeod, C. J. (2021). Shear Zone Development in Serpentinized Mantle: Implications for the Strength of Oceanic Transform Faults. *Journal of Geophysical Research: Solid Earth*, *126*(5). https://doi.org/10.1029/2020JB020763

Crameri, F., Lithgow-Bertelloni, C. R., & Tackley, P. J. (2017). The dynamical control of subduction parameters on surface topography. *Geochemistry, Geophysics, Geosystems*, *18*(4), 1661–1687. https://doi.org/10.1002/2017GC006821

Cundall, P. A. (1989). Numerische Simulation der Lokalisierung in reibungsbehaftetem Material. *Ingenieur-Archiv*, *59*, 148–159.

Dewey, J. F., Helman, M. L., Knott, S. D., Turco, E., & Hutton, D. H. W. (1989). Kinematics of the western Mediterranean. *Geological Society, London, Special Publications*, *45*(1), 265–283.

Dilek, Y. (2003). Ophiolite concept and its evolution. *Special Paper of the Geological Society of America*, *373*, 1–16. https://doi.org/10.1130/0-8137-2373-6.1

Duretz, T., Agard, P., Yamato, P., Ducassou, C., Burov, E. B., & Gerya, T. V. (2016). Thermo-mechanical modeling of the obduction process based on the Oman Ophiolite case. *Gondwana Research*, *32*, 1–10. https://doi.org/10.1016/J.GR.2015.02.002

Eaton, S., & Robertson, A. (1993). The Miocene Pakhna Formation, southern Cyprus and its relationship to the Neogene tectonic evolution of the Eastern Mediterranean. In *Sedimentary Geology* (Vol. 86).

Ergün, M., Okay, S., Sari, C., Oral, E. Z., Ash, M., Hall, J., & Miller, H. (2005). Gravity anomalies of the Cyprus Arc and their tectonic implications. *Marine Geology*, *221*(1–4), 349–358. https://doi.org/10.1016/j.margeo.2005.03.004

Escartín, J., Hirth, G., & Evans, B. (2001). Strength of slightly serpentinized peridotites: Implications for the tectonics of oceanic lithosphere. In *Geology* (Issue 11). www.geosociety.org/pubs/ft2001.htm.

Evans, A. D., Teagle, D. A. H., Craw, D., Henstock, T. J., & Falcon-Suarez, I. H. (2021). Uplift and Exposure of Serpentinized Massifs: Modeling Differential Serpentinite Diapirism and Exhumation of the Troodos Mantle Sequence, Cyprus. *Journal of Geophysical Research: Solid Earth*, *126*(6). https://doi.org/10.1029/2020JB021079

Feld, C., Mechie, J., Hübscher, C., Hall, J., Nicolaides, S., Gurbuz, C., Bauer, K., Louden, K., & Weber, M. (2017). Crustal structure of the Eratosthenes Seamount, Cyprus and S. Turkey from an amphibian wide-angle seismic profile. *Tectonophysics*, *700–701*, 32–59. https://doi.org/10.1016/j.tecto.2017.02.003

Fernandes, R. M. S., Ambrosius, B. A. C., Noomen, R., Bastos, L., Wortel, M. J. R., Spakman, W., & Govers, R. (2003). The relative motion between Africa and Eurasia as derived from ITRF2000 and GPS data. *Geophysical Research Letters*, *30*(16), 1828. https://doi.org/10.1029/2003GL017089

Geological Map of Cyprus. - ESDAC - European Commission. (n.d.). Retrieved January 26, 2024, from https://esdac.jrc.ec.europa.eu/content/geological-map-cyprus

Goetze, C., & Evans, B. (1979). Stress and temperature in the bending lithosphere as constrained by experimental rock mechanics. *Geophysical Journal International*, *59*(3), 463–478. https://doi.org/10.1111/J.1365-246X.1979.TB02567.X

Guillot, S., Schwartz, S., Reynard, B., Agard, P., & Prigent, C. (2015). Tectonic significance of serpentinites. In *Tectonophysics* (Vol. 646, pp. 1–19). Elsevier B.V. https://doi.org/10.1016/j.tecto.2015.01.020

Harrison, R. W., Newell, W. L., Batihanli, H., Panayides, I., McGeehin, J. P., Mahan, S. A., Özhür, A., Tsiolakis, E., & Necdet, M. (2004). Tectonic framework and Late Cenozoic tectonic history of the northern part of Cyprus: Implications for earthquake hazards and regional tectonics. *Journal of Asian Earth Sciences*, *23*(2), 191–210. https://doi.org/10.1016/S1367-9120(03)00095-6

Harrison, R. W., Tsiolakis, E., Stone, B. D., Lord, A., Mcgeehin, J. P., Mahan, S. A., & Chirico, P. (2013). Late pleistocene and holocene uplift history of cyprus: Implications for active tectonics along the southern margin of the anatolian microplate. *Geological Society Special Publication*, *372*(1), 561–584. https://doi.org/10.1144/SP372.3

Hawkins, J. W. (2003). Geology of supra-subduction zones-Implications for the origin of ophiolites. *Special Paper of the Geological Society of America*, *373*(227–268).

Hernández-Molina, F. J., Hüneke, H., Rodríguez-Tovar, F. J., Ng, Z. L., Llave, E., Mena, A., Gibb, A., Chiarella, D., Sammartino, S., & de la Vara, A. (2022). Eocene to middle Miocene contourite deposits in Cyprus: A record of Indian Gateway evolution. *Global and Planetary Change*, *219*. https://doi.org/10.1016/j.gloplacha.2022.103983

Hess, H. H. (1965). Mid-oceanic ridges and tectonics of the sea-floor. In *Submarine geology and geophysics* (Vol. 17, pp. 317–333). Butterworths London.

Hu, J., & Gurnis, M. (2020). Subduction Duration and Slab Dip. *Geochemistry, Geophysics, Geosystems*, *21*(4). https://doi.org/10.1029/2019GC008862

Huangfu, P., Wang, Y., Cawood, P. A., Li, Z. H., Fan, W., & Gerya, T. V. (2016). Thermo-mechanical controls of flat subduction: Insights from numerical modeling. *Gondwana Research*, *40*, 170–183. https://doi.org/10.1016/J.GR.2016.08.012

Inwood, J., Anderson, M. W., Morris, A., & Robertson, A. H. F. (2009). Successive structural events in the Hatay ophiolite of southeast Turkey: Distinguishing oceanic, emplacement and post-emplacement phases of faulting. *Tectonophysics*, *473*(1–2), 208–222. https://doi.org/10.1016/J.TECTO.2008.10.037

Jarrard, R. D. (1986). Relations among subduction parameters. *Reviews of Geophysics*, *24*(2), 217–284.

Jordán, T. E., Isacks, B. L., Allmendinger, R. W., Brewer, J. A., Ramos, V. A., & Ando, C. J. (1983). Andean tectonics related to geometry of subducted Nazca plate. *Geological Society of America Bulletin*, *94*(3), 341–361.

Juteau, T. (2003). Identification of a mantle unit in ophiolites: A major step in the evolution of the ophiolite concept. *Special Paper of the Geological Society of America*, *373*, 31–53. https://doi.org/10.1130/0-8137-2373-6.31

Karato, S.-I., Paterson, M. S., & FitzGerald, J. D. (1986). Rheology of synthetic olivine aggregates: Influence of grain size and water. *Journal of Geophysical Research*, *91*(B8), 8151. https://doi.org/10.1029/jb091ib08p08151

Kempler, D. (1998). 53. Eratosthenes seamount: the possible spearhead of incipient continental collision in the eastern Mediterranean. *Proc Ocean Drill Prog. Sci Res*, *160*, 709–721.

Kinnaird, T. C., & Robertson, A. H. F. (2013). Tectonic and sedimentary response to subduction and incipient continental collision in southern cyprus, easternmost mediterranean region. *Geological Society Special Publication*, *372*(1), 585–614. https://doi.org/10.1144/SP372.10

Kinnaird, T. C., Robertson, A. H. F., & Morris, A. (2011). Timing of uplift of the Troodos Massif (Cyprus) constrained by sedimentary and magnetic polarity evidence. *Journal of the Geological Society*, *168*(2), 457–470. https://doi.org/10.1144/0016-76492009-150

Klein, F., Bach, W., Humphris, S. E., Kahl, W. A., Jöns, N., Moskowitz, B., & Berquó, T. S. (2014). Magnetite in seafloor serpentinite-Some like it hot. *Geology*, *42*(2), 135–138. https://doi.org/10.1130/G35068.1

Koptev, A., Nettesheim, M., & Ehlers, T. A. (2022). Plate corner subduction and rapid localized exhumation: Insights from 3D coupled geodynamic and geomorphological modelling. *Terra Nova*, *34*(3), 210–223. https://doi.org/10.1111/TER.12581

Krijgsman, W., Hilgen, F. J., Raffi, I., Sierro, F. J., & Wilson, D. S. (1999). Chronology, causes and progression of the Messinian salinity crisis. *Nature 1999 400:6745*, *400*(6745), 652–655. https://doi.org/10.1038/23231

Lapierre, H., Bosch, D., Narros, A., Mascle, G. H., Tardy, M., & Demant, A. (2007). The Mamonia Complex (SW Cyprus) revisited: Remnant of Late Triassic intra-oceanic volcanism along the Tethyan southwestern passive margin. *Geological Magazine*, *144*(1), 1–19. https://doi.org/10.1017/S0016756806002937

Le Pourhiet, L., Burov, E., & Moretti, I. (2004). Rifting through a stack of inhomogeneous thrusts (the dipping pie concept). *Tectonics*, *23*(4). https://doi.org/10.1029/2003TC001584

Livermore, R. A., Vine, F. J., & Smith, A. G. (1984). Plate motions and the geomagnetic field—II. Jurassic to Tertiary. *Geophysical Journal International*, *79*(3), 939–961.

Mackenzie, G. D., Maguire, P. K. H., Coogan, L. A., Khan, M. A., Eaton, M., & Petrides, G. (2006). Geophysical constraints on the crustal architecture of the Troodos ophiolite: Results from the IANGASS project. *Geophysical Journal International*, *167*(3), 1385–1401. https://doi.org/10.1111/j.1365-246X.2006.03144.x

Mackwell, S. J., Zimmerman, M. E., & Kohlstedt, D. L. (1998). High-temperature deformation of dry diabase with application to tectonics on Venus. *Journal of Geophysical Research: Solid Earth*, *103*(1), 975–984. https://doi.org/10.1029/97jb02671

MacLeod, C. J., Johan Lissenberg, C., & Bibby, L. E. (2013). "Moist MORB" axial magmatism in the Oman ophiolite: The evidence against a mid-ocean ridge origin. *Geology*, *41*(4), 459–462.

Maffione, M., van Hinsbergen, D. J. J., de Gelder, G. I. N. O., van der Goes, F. C., & Morris, A. (2017). Kinematics of Late Cretaceous subduction initiation in the Neo-Tethys Ocean reconstructed from ophiolites of Turkey, Cyprus, and Syria. *Journal of Geophysical Research: Solid Earth*, *122*(5), 3953–3976. https://doi.org/10.1002/2016JB013821

Magaritz, M., & Taylor, H. P. (1974). OXYGEN AND HYDROGEN ISOTOPE STUDIES OF SERPENTINIZATION IN THE TROODOS OPHIOLITE COMPLEX, CYPRUS *. In *Earth and Planetary Science Letters* (Vol. 23).

Malpas, J., Xenophontos, C., & Williams, D. (1992). *The Ayia Varvara Formation of SW Cyprus: a product of complex collisional tectonics*. 193–211.

Martin, B., & Fyfe, W. S. (1970). Some experimental and theoretical observations on the kinetics of hydration reactions with particular reference to serpentinization. *Chemical Geology*, *6*(C), 185–202. https://doi.org/10.1016/0009-2541(70)90018-5

McCallum, J. E. (1989). *Sedimentation and tectonics of the Plio-Pleistocene of Cyprus*. University of Edinburgh.

McCallum, J. E., & Robertson, A. H. F. (1995). Sedimentology of two fan-delta systems in the Pliocene-Pleistocene of the Mesaoria Basin, Cyprus. In *SEDIMENTARY GEOLOGY ELSEVIER Sedimentary Geology* (Vol. 98).

McPhee, P. J., & van Hinsbergen, D. J. J. (2019). Tectonic reconstruction of Cyprus reveals Late Miocene continental collision of Africa and Anatolia. *Gondwana Research*, *68*, 158–173. https://doi.org/10.1016/j.gr.2018.10.015

Mével, C. (2003). Serpentinisation des péridotites abysales aux dorsales océaniques. *Comptes Rendus - Geoscience*, *335*(10–11), 825–852. https://doi.org/10.1016/j.crte.2003.08.006

Morag, N., Haviv, I., & Katzir, Y. (2016). From ocean depths to mountain tops: Uplift of the Troodos ophiolite (Cyprus) constrained by low-temperature thermochronology and geomorphic analysis. *Tectonics*, *35*(3), 622–637. https://doi.org/10.1002/2015TC004069

Morris, A. (1996). A review of palaeomagnetic research in the Troodos ophiolite, Cyprus. *Geological Society, London, Special Publications*, *105*(1), 311–324.

Morris, A., & Maffione, M. (2016). Is the Troodos ophiolite (Cyprus) a complete, transform fault-bounded Neotethyan ridge segment? *Geology*, *44*(3), 199–202. https://doi.org/10.1130/G37529.1

Mukasa, S. B., & Ludden, J. N. (1987). *Uranium-lead isotopie ages of plagiogranites from the Troodos ophiolite, Cyprus, and their tectonic significance*. http://pubs.geoscienceworld.org/gsa/geology/article-pdf/15/9/825/3510149/i0091-7613-15-9-825.pdf

Murton, B. J., & Cass, I. G. (1986). Western Limassol Forest complex, Cyprus: part of an Upper Cretaceous leaky transform fault. *Geology*, *14*(3), 255–258.

Nuriel, P., Katzir, Y., Abelson, M., Valley, J. W., Matthews, A., Spicuzza, M. J., & Ayalon, A. (2009). Fault-related oceanic serpentinization in the Troodos ophiolite, Cyprus: Implications for a fossil oceanic core complex. *Earth and Planetary Science Letters*, *282*(1–4), 34–46. https://doi.org/10.1016/j.epsl.2009.02.029

Osozawa, S., Shinjo, R., Lo, C. H., Jahn, B. M., Hoang, N., Sasaki, M., Ishikawa, K., Kano, H., Hoshi, H., Xenophontos, C., & Wakabayashi, J. (2012). Geochemistry and geochronology of the troodos ophiolite: An ssz ophiolite generated by subduction initiation and an extended episode of ridge subduction. *Lithosphere*, *4*(6), 497–510. https://doi.org/10.1130/L205.1

Oufi, O., Cannat, M., & Horen, H. (2002). Magnetic properties of variably serpentinized abyssal peridotites. *Journal of Geophysical Research: Solid Earth*, *107*(B5). https://doi.org/10.1029/2001jb000549

Poole, A. J., & Robertson, A. H. F. (1991). Quaternary uplift and sea-level change at an active plate boundary, Cyprus. In *Journal ofthe Geological Society* (Vol. 148). https://www.lyellcollection.org

Poole, A. J., & Robertson, A. H. F. (1998). Pleistocene Fanglomerate deposition of the Troodos Ophiolite, Cyprus. In *Scientific Results* (Vol. 160).

Porkoláb, K., Duretz, T., Yamato, P., Auzemery, A., & Willingshofer, E. (2021). Extrusion of subducted crust explains the emplacement of far-travelled ophiolites. *Nature Communications*, *12*(1). https://doi.org/10.1038/s41467-021-21866-1

Prichard, H. M. (1979). A Petrographic Study of the Process of Serpentinisation in Ophiolites and the Ocean Crust. In *Contrib. Mineral. Petrol* (Vol. 68).

Pusok, A. E., Stegman, D. R., & Kerr, M. (2021). The effect of sediments on the dynamics and accretionary style of subduction margins. *Solid Earth Discussions*, *2021*, 1–30.

Reilinger, R. E., McClusky, S. C., Oral, M. B., King, R. W., Toksoz, M. N., Barka, A. A., Kinik, I., Lenk, O., & Sanli, I. (1997). Global Positioning System measurements of present-day crustal movements in the Arabia-Africa-Eurasia plate collision zone. *Journal of Geophysical Research: Solid Earth*, *102*(B5), 9983–9999. https://doi.org/10.1029/96jb03736

Ring, U., & Pantazides, H. (2019). The Uplift of the Troodos Massif, Cyprus. *Tectonics*, *38*(8), 3124–3139. https://doi.org/10.1029/2019TC005514

Robertson, A. H. F. (1977). *Tertiary uplift history of the Troodos massif, Cyprus*. http://pubs.geoscienceworld.org/gsa/gsabulletin/article-pdf/88/12/1763/3418490/i0016-7606-88-12-1763.pdf

Robertson, A. H. F. (1990). Tectonic evolution of Cyprus. *Troodos 1987. Symposium*, 235–250.

Robertson, A. H. F. (1998a). Mesozoic-Tertiary tectonic evolution of the easternmost Mediterranean area: integration of marine and land evidence. *Proceedings of the Ocean Drilling Program, Scientific Results, Vol. 160; Chapter 54*.

Robertson, A. H. F. (1998b). Tectonic significance of the Eratosthenes Seamount: a continental fragment in the process of collision with a subduction zone in the eastern Mediterranean (Ocean Drilling Program Leg 160). In *Tectonophysics* (Vol. 298).

Robertson, A. H. F., & Kinnaird, T. C. (2016). Structural development of the central Kyrenia Range (north Cyprus) in its regional setting in the eastern Mediterranean region. *International Journal of Earth Sciences*, *105*, 417–437.

Robertson, A. H. F., & Woodcock, N. H. (1980). Strike-slip related sedimentation in the Antalya Complex, Southwest Turkey. *Sedimentation in Oblique-Slip Mobile Zones*, 127–145.

Rouchy, J. M., Orszag-Sperber, F., Blanc-Valleron, M.-M., Pierre, C., Rivie Áre, M., Combourieu-Nebout, N., & Panayides, I. (2001). *Paleoenvironmental changes at the Messinian±Pliocene boundary in the eastern Mediterranean (southern Cyprus basins): signi®cance of the Messinian Lago-Mare*. www.elsevier.com/locate/sedgeo

Rouméjon, S., & Cannat, M. (2014). Serpentinization of mantle-derived peridotites at mid-ocean ridges: Mesh texture development in the context of tectonic exhumation. *Geochemistry, Geophysics, Geosystems*, *15*(6), 2354–2379. https://doi.org/10.1002/2013GC005148

Schuiling, R. D. (2011). Troodos: A Giant Serpentinite Diapir. *International Journal of Geosciences*, *02*(02), 98–101. https://doi.org/10.4236/ijg.2011.22010

Schwarzenbach, E. M., Caddick, M. J., Beard, J. S., & Bodnar, R. J. (2016). Serpentinization, element transfer, and the progressive development of zoning in veins: evidence from a partially serpentinized harzburgite. *Contributions to Mineralogy and Petrology*, *171*(1), 1–22. https://doi.org/10.1007/s00410-015-1219-3

Searle, M. P., & Cox, J. (2002). Subduction zone metamorphism during formation and emplacement of the Semail ophiolite in the Oman Mountains. *Geological Magazine*, *139*(3), 241–255. https://doi.org/10.1017/S0016756802006532

Şengör, A. M. C., & Yilmaz, Y. (1981). Tethyan evolution of Turkey: a plate tectonic approach. *Tectonophysics*, *75*(3–4), 181–241.

Shelton, A. W. (1993). Troodos revisited: the Mount Olympus gravity anomaly. *Geological Society, London, Special Publications*, *76*(1), 197–212.

Skelton, A. D. L., & Valley, J. W. (2000). The relative timing of serpentinisation and mantle exhumation at the ocean–continent transition, Iberia: constraints from oxygen isotopes. *Earth and Planetary Science Letters*, *178*(3–4), 327–338. https://doi.org/10.1016/S0012-821X(00)00087-X

Spray, J. G., & Roddick, J. C. (1981). Evidence for Upper Cretaceous transform fault metamorphism in West Cyprus. *Earth and Planetary Science Letters*, *55*(2), 273–291.

Steinmann, G. (1927). Der ophiolitischen Zonen in der mediterranean Kettengebirgen. *14th International Geological Congress in Madrid*, *2*, 638–667.

Stow, D. A. V, Braakenburg, N. E., & Xenophontos, C. (1995). The Pissouri Basin fan-delta complex, southwestern Cyprus. In *SEDIMENTARY GEOLOGY ELSEVIER Sedimentary Geology* (Vol. 98).

Symeou, V., Homberg, C., Nader, F. H., Darnault, R., Lecomte, J. C., & Papadimitriou, N. (2018). Longitudinal and Temporal Evolution of the Tectonic Style Along the Cyprus Arc System, Assessed Through 2-D Reflection Seismic Interpretation. *Tectonics*, *37*(1), 30–47. https://doi.org/10.1002/2017TC004667

Tan, E., Lavier, L. L., Van Avendonk, H. J. A., & Heuret, A. (2012). The role of frictional strength on plate coupling at the subduction interface. *Geochemistry, Geophysics, Geosystems*, *13*(10). https://doi.org/10.1029/2012GC004214

Wada, I., Wang, K., He, J., & Hyndman, R. D. (2008). Weakening of the subduction interface and its effects on surface heat flow, slab dehydration, and mantle wedge serpentinization. *Journal of Geophysical Research: Solid Earth*, *113*(4). https://doi.org/10.1029/2007JB005190

Wakabayashi, J., & Dilek, Y. (2000). Spatial and temporal relationships between ophiolites and their metamorphic soles: A test of models of forearc ophiolite genesis. *Special Paper of the Geological Society of America*, *349*, 53–64. https://doi.org/10.1130/0-8137-2349-3.53

Whitechurch, H., Juteau, T., & Montigny, R. (1984). *Role of the Eastern Mediterranean ophiolites (Turkey, Syria, Cyprus) in the history of the Neo-Tethys*. https://www.lyellcollection.org

Woelki, D., Regelous, M., Haase, K. M., & Beier, C. (2019). Geochemical mapping of a paleo-subduction zone beneath the Troodos Ophiolite. *Chemical Geology*, *523*, 1–8. https://doi.org/10.1016/j.chemgeo.2019.05.041

Yamato, P., Agard, P., Burov, E., Le Pourhiet, L., Jolivet, L., & Tiberi, C. (2007). Burial and exhumation in a subduction wedge: Mutual constraints from thermomechanical modeling and natural P-T-t data (Schistes Lustrés, western Alps). *Journal of Geophysical Research: Solid Earth*, *112*(7). https://doi.org/10.1029/2006JB004441

Yamato, P., Burov, E., Agard, P., Le Pourhiet, L., & Jolivet, L. (2008). HP-UHP exhumation during slow continental subduction: Self-consistent thermodynamically and thermomechanically coupled model with application to the Western Alps. *Earth and Planetary Science Letters*, *271*(1–4), 63–74. https://doi.org/10.1016/j.epsl.2008.03.049

Young, E. C. (2014). *Volcanology of the Troodos Ophiolite (Cyprus) and mechanisms of accretion of the upper oceanic crust*.

Zomeni, S. L. (1977). *Hydrogeology of Central Mesaoria - Cyprus*. University of London.